Recent progress on strategies to improve the high-voltage stability of layered-oxide cathode materials for sodium-ion batteries

Song, Tengfei; Kendrick, Emma

DOI:
10.1088/2515-7639/abf545

Document Version
Publisher's PDF, also known as Version of record

Citation for published version (Harvard):
Song, T & Kendrick, E 2021, 'Recent progress on strategies to improve the high-voltage stability of layered-oxide cathode materials for sodium-ion batteries', *JPhys Materials*, vol. 4, no. 3, 032004. https://doi.org/10.1088/2515-7639/abf545

JPhys Materials

TOPICAL REVIEW • OPEN ACCESS

Recent progress on strategies to improve the high-voltage stability of layered-oxide cathode materials for sodium-ion batteries

IOP Publishing J. Phys. Mater. 4 (2021) 032004 https://doi.org/10.1088/2515-7639/abf545

Journal of Physics: Materials

OPEN ACCESS

RECEIVED
16 November 2020

REVISED
10 March 2021

ACCEPTED FOR PUBLICATION
6 April 2021

PUBLISHED
21 April 2021

TOPICAL REVIEW

Recent progress on strategies to improve the high-voltage stability of layered-oxide cathode materials for sodium-ion batteries

Tengfei Song and Emma Kendrick*

School of Metallurgy and Materials, University of Birmingham, Edgbaston, Birmingham B15 2TT, United Kingdom
* Author to whom any correspondence should be addressed.

E-mail: E.Kendrick@bham.ac.uk

Keywords: sodium-ion battery, layered-oxide cathode, degradation mechanisms, optimization strategies, NIB

Abstract

Sodium-ion batteries offer a low-cost sustainable alternative to current lithium-ion batteries and can be made on the same manufacturing lines. The sustainability arises from the low cost, reduction in the use of critical elements and strategic materials, and potential long-life. To maximize their potential, higher energy density batteries are required, this can be achieved in part through the stabilization of higher voltage cathode materials. In this review we summarize the failure and degradation processes associated with the high capacity and higher voltage layered oxide cathode materials. Material crystal structure rearrangements, electrolyte oxidation, particle cracking and reactive surfaces form most of the degradation mechanisms. Strategies to overcome these processes are discussed in detail, and the synergistic requirements to stabilize the materials structure and the interfaces highlighted. The importance of surface engineering in future materials design is emphasized.

1. Introduction

Lithium-ion batteries (LIBs) are the most mature electrochemical energy storage technology and have been incorporate into a diverse array of applications ranging from consumer electronics, electric vehicles to large energy grids since its commercialization by Sony in the 1990s. However, the relatively low abundance and non-uniform global distribution of lithium, cobalt and more recently nickel resources have raised concerns about the sustainable supply to meet the future market demand, especially with the tremendous development of electric vehicles and stationary energy storage. It should be noted that the lithium (or sodium) raw material cost is not typically the controlling cost factor due to their limited mass content in the cathode materials and electrolyte. The availability and the fluctuation in costs of the transition metals, particularly cobalt and nickel are more of a concern. This concern that has prompted the search for low-cost alternatives to LIB [1, 2].

Among those various potential technologies, sodium-ion batteries (NIBs) are one of the most promising substitutes or complements for LIBs due to the abundance, easy accessibility, and low cost of sodium (e.g. the cost of Na_2CO_3 is about 25–30 times lower than that of Li_2CO_3) [3, 4]. Sodium and lithium are both alkali metals, therefore there are many similarities in their chemical and electrochemical properties, which enables NIBs and LIBs to use the same cell design and manufacturing lines. All these similarities suggest that NIB is a 'drop-in' or direct substitute technology for LIBs [5]. However, compared with lithium ions (0.76 Å), the larger ionic radius of sodium ions (1.02 Å) induces multiple structural evolutions during Na^+ insertion/extraction, resulting in deteriorating host crystal structures and unsatisfactory cycling stability [6]. Additionally, the higher atomic weight of Na (Na 23 g mol^{-1} vs Li 6.9 g mol^{-1}) and higher standard electrochemical potential (Na −2.71 V vs Li −3.04 V with respect to standard hydrogen electrode SHE) make it difficult for NIBs to surpass LIBs in terms of energy density [7, 8]. Therefore, though the NIBs present the advantage of raw materials cost, this advantage is offset by their lower energy density, which may result in a higher cost per watt-hour, further impeding the commercial application of NIBs. Thus, new low-cost and higher capacity NIBs anode and cathodes are required, which when manufactured into a cell will have a long

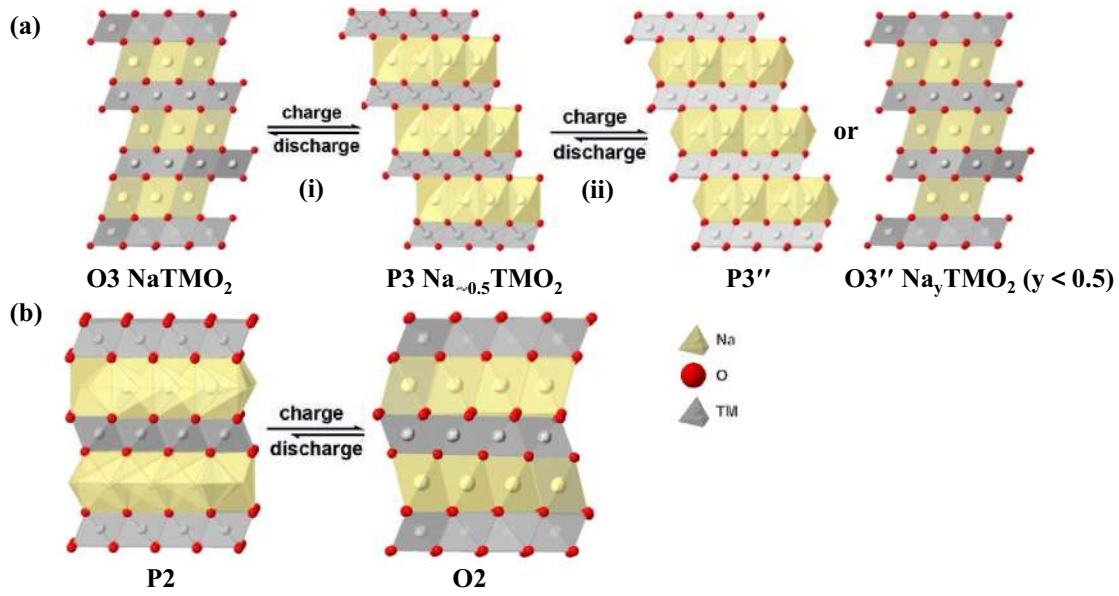

Figure 1. Schematic illustration of typical structural evolution during charge/discharge of (a) O3-, and (b) P2-phase layered oxides.

cycle and calendar life. This will effectively reduce the cost of energy (Wh) per cycle and further aid adoption into new markets.

Given that critical battery characteristics such as energy density, cycling performance and cost are primarily determined by the cathode materials, efforts have been made to explore new cathode materials for NIBs with a high capacity, stable structure and low cost [9]. Cathode materials for NIBs can be divided into four categories: metal oxides, polyanionic compounds, Prussian blue analogues, and organic compounds [10]. This review focuses upon the layered oxide cathodes, as currently these materials offer the most advanced chemistry for obtaining the gravimetric and volumetric energy densities required for applications such as transport, e-bikes, e-scooters, small electric vehicles. These cathodes once incorporated into a full cell configuration may rival $LiFePO_4$ cells in terms of performance properties and enter markets where alternatives or substitutes to lithium are required or can be used.

Among these candidates, Na_xTMO_2-layered oxides ($0 < x \leqslant 1$, TM refers to a transition metal, typically; Fe, Ni, Co, and Mn), which can be grouped into O3-type and P2-type crystal structure families, and are considered as one of the most appealing structure types because of their low cost, high theoretical capacity, appropriate operating potential and simple synthesis processes [7, 9–12]. However, these types of crystal structure often suffer from complex phase transformations during the Na^+ extraction/insertion process compared to their Li analogues, especially when charged to higher cut-off voltage [13–16]. For P2 layered materials, irreversible P2-O2 phase transition will occur when charged to 4.2 V vs Na/Na^+ (figure 1(b)) [17–20]. O3-type oxides commonly undergo more complex phase transitions than the P2-type oxides. Most of the studied O3-$NaTMO_2$ materials experience two major phase transitions, namely (figure 1(a)) (i) reversible O3 $NaTMO_2 \Leftrightarrow$ P3 $Na_{\sim 0.5}TMO_2$ and (ii) irreversible P3 $Na_{\sim 0.5}TMO_2 - X\ Na_yMO_2$, where y and the high voltage phase X varies with the nature of TM and the voltage window [21]. Examples are illustrated by the crystal structural changes from O3–O′3–P3–P′3–P3″ for $NaNi_{0.5}Mn_{0.5}O_2$ [22], and O3–O′3–P3–O3″ for $NaNi_{0.60}Fe_{0.25}Mn_{0.15}O_2$ [23]. Such irreversible phase transitions occurring under high voltage easily led to crystal structural collapse and thus display a rapid capacity degradation upon cycling. As a compromise measure, only 0.5–0.6 Na^+ per formula unit are removed to maintain the crystal structural stability, leading to a lower observed specific capacities, which are lower than one of the near commercial NIB polyanionic cathodes $Na_3V_2(PO_4)_2F_3$ (NVPF) [21, 23–25].

In recent years, efforts have been devoted to further improve the structural stability and electrochemical properties of layered materials under higher operation voltage with the aim to narrow the gap between the energy density of NIB and LIB. Despite such efforts, the capacity and cycling stability of Na_xTMO_2-layered oxide materials still require further improvements. In this review, we will focus on the recent progress in the layered cathode materials by identifying the main causes of failure under high-voltage operation and the corresponding strategies to prevent this. A summary of these processes is shown in figure 2.

Figure 2. Overview on proposed degradation mechanisms for sodium layered oxide materials under high voltage operations.

2. Main causes of failure under high-voltage operation

2.1. Phase transitions and induced bulk degradation

Though various reasons contribute to the performance degradation under high-voltage operation, the irreversible bulk phase transitions are most prominent. From the perspective of crystal structure, these multiphase transformations originate from the Na^+ vacancy ordering and the MO_2 layers shifting to different sites. This inevitably causes large expansion and volume shrinkage as well as sluggish kinetics, which are unfavourable to the structural stability and rate performance, during the cycling process [6, 26]. From the macroscopic particle point of view, the phase transition induced volume change not only causes the collapse of active layered crystal structure but also affects the macroscopic properties of the particles. The resulting stress and strain induce cracks within a single particle. The bulk cracks lead to poor electronic conduction, TM dissolution, surface corrosion, and electrolyte consumption [27]. The unwanted side reactions, or parasitic reaction, become more prevalent at higher voltages, and increasing Na^+ extraction. For example, $NaNi_{1/3}Fe_{1/3}Mn_{1/3}O_2$ illustrates high reversibility through an O3–P3–P3–O3 sequence during cycling in the voltage range of 2.0–4.0 V, and the R-3 m layered structure remained intact after more than 100 cycles. However, when the cut-off voltage is higher than 4.0 V, a new nonequilibrium O3′ monoclinic phase is observed along with a significant contraction in d-spacing and *c* axis, which leads to severe deterioration in structural stability and cycling performance [28, 29]. Stabilizing, eliminating, suppressing, or delaying this high voltage phase transition and extending the solid solution zone are critical to further improve the structural stability of sodium layered oxide materials at high charge cut-off voltages.

2.2. Surface related chemical degradation

In addition to structural stability challenges, the interface instability also requires further development to enable practical high-voltage NIBs. The interface issues include surface instability in air and interfacial reactions between deep-charged cathode and electrolyte above 4.2 V.

2.2.1. Surface instability in air and moisture

Due to the larger spacing between transition metal layers than the lithium analogues, the sodiated transition metal oxides are highly hygroscopic, and they will readily react with water and CO_2 to form NaOH and Na_2CO_3 on the particle surface even with brief exposure to ambient air [30, 31]. These impurities can severely accelerate the structural degradation of cathode material, diminishing the electrochemical performance while cycling. The main processes are: (a) the surface becomes more basic, which leads to difficulty in producing stable slurries and uniform electrode casting [32]; (b) the formed NaOH and Na_2CO_3 are insulating and cause poor electronic conduction, which also leads to an increase in cell polarization and decrease in capacity; (c) the intercalated water molecules within the layers will trigger side reactions with electrolyte through the following reactions: $NaPF_6 \rightarrow NaF + PF_5$, $PF_5 + H_2O \rightarrow POF_3 + 2HF$ [33–36]. On one side, the as-formed HF tends to react with the surface by-products such as Na_2CO_3 to form further NaF and H_2O. On the other side, HF will aggressively attack the TM oxides, inducing the transition metal dissolution and forming TM fluorides on the cathode surface, which result in irreversible active mass loss [37–39].

2.2.2. Interfacial reactions between deep-charged cathode and electrolyte

The interfacial stability between the cathode and electrolyte plays a crucial role on the ultimate electrochemical performance for a cell. Under ideal conditions, the commonly used nonaqueous electrolytes for NIBs ($NaPF_6$ or $NaClO_4$ salt in carbonate-based solvents) are not thought to degrade upon the surface or form a particular cathode electrolyte interface (CEI). However, during cycling, and at high voltages surface films have been observed. Particularly at higher voltages cycling limits. It is thought that at the higher voltages, particularly above ≈4.2 V, the electrolyte may become thermodynamically unstable, and oxidize at the surface causing an insulating interface layer, which has negative effects upon the performance properties [40].

There are several possible causes of these higher voltage (>4.2 V vs Na/Na^+) parasitic oxidative reactions at the cathode interface. (a) Oxygen loss from the cathode surface which subsequently reacts with the electrode, and (b) cathode-electrolyte side reactions induce oxygen loss from the cathode lattice. Whichever mechanism is responsible for the oxidation at the surface of the cathode, several subsequent reactions occur including the reduction of the transition metals. This metal dissolution from the lattice causes surface crystal structure reconstruction and the dissolved transition metal ions can also migrate through the electrolyte and deposit on the anode to form a film, increasing the impedance of the cell. Meanwhile, the intragranular nano cracks caused by the TMs leaching in the outer layer can generate more fresh oxide surfaces that can further be involved in these side reactions, this 'domino effect' contributes to cascade failure of cells [41–43]. Furthermore, the decay observed from this sequential reduction-dissolution process will exponentially aggravate when operating at higher cut-off voltage or elevated temperatures. Given the general instability of the surface, engineering a robust interface between cathode/electrolyte is essential for building a battery with superior cycling stability.

In short, the lower standard electrochemical potential of sodium-ion electrode materials determines that they must operate under higher voltages to pursue equivalent energy density to their lithium counterpart; however, complex phase transitions and severe interfacial reactions at high voltages can inevitably reduce its service life. This inherent contradiction makes it extremely difficult to develop sodium-containing layered oxide materials with simultaneous high energy density and long cycle life and has become a significant obstacle to the practical application of these layered oxides in a NIB.

3. Strategies for high voltage stabilization

3.1. Layered oxide material structure and composition

It is acknowledged that Na^+/vacancy ordered superstructures originate from strong Na^+–Na^+ interactions in the alkali metal layers. This, along with charge ordering in the transition metal layers, can introduce several phase changes, which result in voltage plateaus. The Na^+ transport kinetics at the voltages at which these phases changes are reduced, and often these phase changes are only partially reversible for which the consequence is a reduced cycle life. This is in contrast to a solid solution transition (sloping voltage profile), and as no phases changes occur, there is little observed change in the sodium transport kinetics and longer cycle lives are observed [44]. As such, constructing a cathode material without Na^+/vacancy ordering during cycling by rational compositional design, could be one promising strategy for developing high energy density NIBs (high entropy materials). In 2015, Toumar *et al* predicted the existence of stable Na-vacancy ordering compounds through thorough DFT computation [45]. Wang *et al* found that such Na^+/vacancy ordering can be avoided by choosing transition metal ions with small differences in ionic radii ($rM_1/rM_2 \leqslant 1.15$) but large differences in redox potentials, for example, in this case, Cr^{3+} and Ti^{4+} were chosen, and successfully co-doped into the crystal structure to reduce the Na^+/vacancy ordering. The P2–$Na_{0.6}(Cr_{0.6}Ti_{0.4})O_2$ is completely disordered at all sodium concentrations and displays long cycle stability with a capacity retention of 94% over 200 cycles at 1 C (76 mAg^{-1}) [44]. In 2018, Guo's group successfully constructed a fully disordered P2–$Na_{2/3}Ni_{1/3}Mn_{1/3}Ti_{1/3}O_2$ material [46]. The electron delocalization is limited by partial substitution of Ti for Mn which have compatible ionic radii very different Fermi levels in the P2-layered oxide. A greater solid solution is observed in the voltage profile, indicating no Na^+-ion/vacancy ordering. As a results high rates and long cycle life were observed (83.9% capacity retention after 500 cycles at 1 C, and 77.5% capacity retention at 20 C, 1 C = 173 mA g^{-1}) with a loading mass of 3–4 mg cm^{-2}. The same conclusion was also drawn by Gutierrez [47], Sung [48], and Zhao [49], who successfully doped metals onto the B site of P2 type–A_xBO_2 to reduce the Na^+-ion/vacancy ordering of $Na_{0.62}Mn_{0.75}Ni_{0.25}O_2$, $Na_{0.67}Co_{1-x}Ti_xO_2$, and $Na_{0.67}Ni_{0.2-x}Mn_{0.8}Mg_xO_2$ and reduce the number of phase transitions occurring during charge and discharge., This resulted in improved sodium diffusion rates and stability of the layered structure upon cycling.

These findings point us towards a new avenue to design layered oxide materials with highly stable structures through controlling the Na^+-ion/vacancy ordering and reducing charge ordering in the transition metal layer. This leads to improved rate capability and long cycle stability of the layered oxides.

3.2. Selective cationic and anion doping into the crystal framework

The irreversible migration of transition metal ions during the charge process triggers a structural distortion, leading to phase reforming and transition, resulting in the observed electrochemical performance fading [50].

To suppress phase transformation (structure changes), many researchers have focused on developing effective structural modifications for practical use in NIBs. Doping elective electrochemically active/inactive elements, such as Li [51], Cu [52–54], Mg [55, 56], Ti [57–60], and Sn [61–66], has been proven as an effective strategy to modify a material's bulk structure properties and improve the high-voltage stability of layered oxides.

3.2.1. Cationic doping

Cationic dopants can be broadly divided into three categories according to the corresponding working mechanisms.

3.2.1.1. Strengthening the bonding between TM and O

The most widely accepted role of element doping in layered oxides is to stabilize the TM slabs through strengthening the bonds between TM and O and thus suppress the host rearrangement and TMO_2 gliding [26]. Chen *et al* found that partial substituted Mn^{4+} by Ti^{4+} in $Na(Ni_{0.4}Fe_{0.2}Mn_{0.4-x}Ti_x)O_2$ can not only lift the working potentials but also improve the reversibility [57]. Huang *et al* systematically investigated the effects of Ti doping on structural modification in O3-type $Na(Fe_{0.25}Ni_{0.25}Mn_{0.5})O_2$ based on experiments and first-principles calculations, and elucidated the corresponding mechanism. They suggested that Ti^{4+} ($3d^\circ$) without d electrons effectively enhances the bonding between transition metals and oxygen by increasing the oxygen electron density, which in turn makes the host structure more stable and lowers the energy barrier of Na^+ migration, leading to a notable enhancement in cycling performance and rate capability of $Na[Ti_{0.03}(Fe_{0.25}Ni_{0.25}Mn_{0.5})_{0.97}]O_2$ [59]. In addition to stabilizing the host structure, Ti^{4+} substitution has also been found to be beneficial to improving stability in air and to water. Tripathi *et al* compared the hydro-stability and surface composition of $Na_{0.9}Cu_{0.22}Fe_{0.30}Mn_{0.48}O_2$ and $Na_{0.9}Cu_{0.22}Fe_{0.30}Mn_{0.43}Ti_{0.05}O_2$ by x-ray photoelectron spectroscopy, found that the Ti^{4+} substituted oxides tend to form a titanium-rich surface which helps reduce the reactivity of the active material with moisture, leading to improved water-stability [67].

Sn^{4+} ($4d^{10}$), a non-transition metal, has a fully filled 4d electron shell, and therefore it cannot interact with oxygen p orbitals, unlike the redox active TMs. This doping effect strengthens the ionic bonding between the remaining transition metals within the lattice and is reflected by the increase in the observed average voltage, the suppression of the high voltage phase and hence the improved cycle life of these materials [62, 68]. Sathiya *et al* synthesized a series of Sn substituted materials $NaNi_{0.5}Mn_{0.5-y}Sn_yO_2$ ($y = 0$–0.5) and found that the Sn substituted material $NaNi_{0.5}Sn_{0.5}O_2$ showed significantly enhanced stability against O3 $\Leftrightarrow$ P3 transformation. This transition did not occur till the removal of 0.5 sodium from the structure as compared to 0.2 for the pristine $NaNi_{0.5}Mn_{0.5}O_2$ material, and the P3 $\Leftrightarrow$ P′3 completely avoided (figures 3(a) and (b)) [63]. Wang *et al* confirmed this conclusion: they synthesized a whole new family of O3-type cathode materials with the general formula $Na_xNi_{x/2}Sn_{1-x/2}O_2$ and found that the phase transition from O3 to P3 was largely delayed by Sn substitution, and the first candidate $Na_{0.7}Ni_{0.35}Sn_{0.65}O_2$ displayed a high average voltage and working potential of 3.7 V (vs Na^+/Na) [62]. Rong *et al* found that Sn-substitution in $Na_{0.67}Ni_{0.33}Mn_{0.67}O_2$ has a triple effect: the formation of O3-stacking, smoothing the charge/discharge voltage profile by inhibiting complex phase transitions, and increasing the average working voltage (3.34 V for $Na_{0.67}Ni_{0.33}Mn_{0.67}O_2$ and 3.60 V for $Na_{0.67}Ni_{0.33}Mn_{0.33}Sn_{0.33}O_2$ vs Na/Na^+) [65]. Other non-redox active elements with empty d orbitals, have also been found to suppress the high voltage phase transition. Mao found that Zn^{2+} doped O3-type $NaNi_{0.2}Fe_{0.35}Mn_{0.45-x}Zn_xO_2$ enhanced the Na^+ diffusion rate, but also reduced the lattice cell variations during Na^+ extraction/insertion, extending the O3-P3 reversible phase transformation region. In addition, it was suggested that the substitution of Zn for Mn can reduce the content of unfavourable Mn^{3+} in the crystal structure and hence improve the cycling stability [69]. Other substitutions, like Ca^{2+}, Zn^{2+} substitution at the Na site has also been shown effective to suppress the formation of these unstable high voltage phases [70, 71].

3.2.1.2. Modulating the interlayer spacing

Another major role of element doping is to modulate the interlayer spacing within the layered oxide crystal structure. It is well known that P2-type oxides process a larger Na layer spacing compared to O3-oxides,

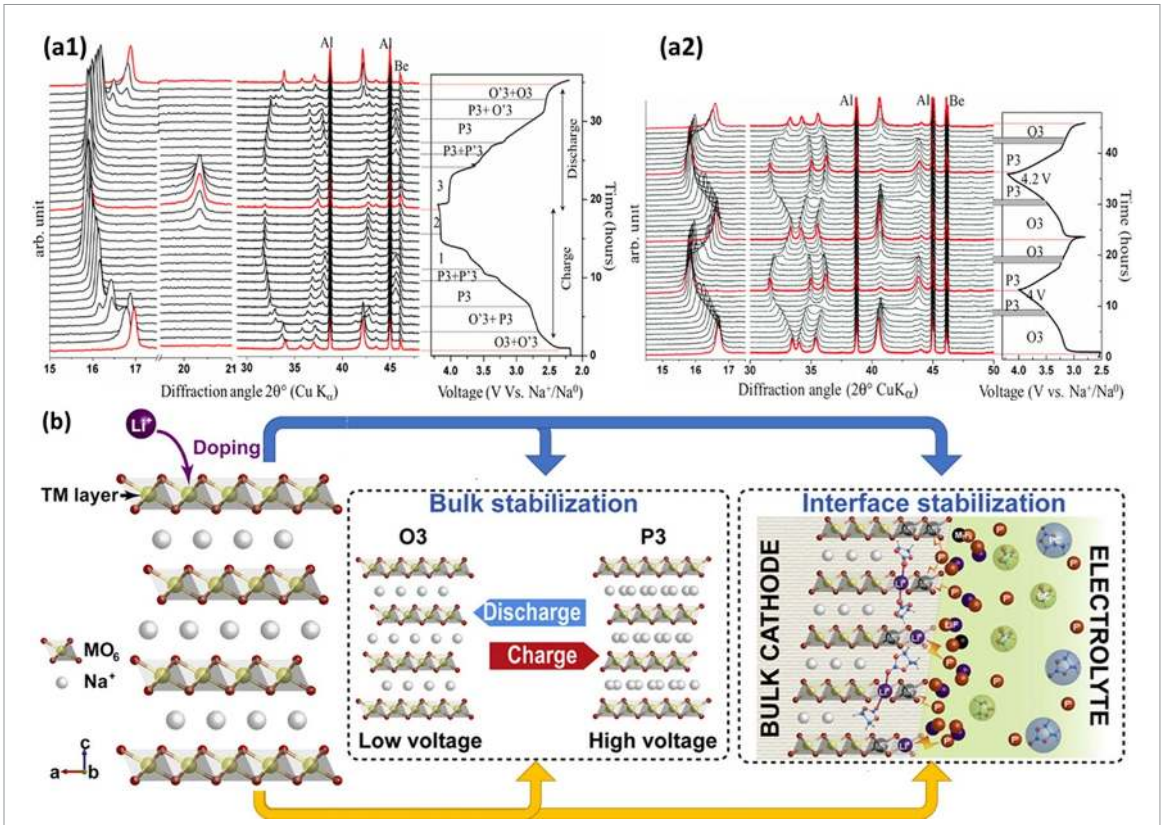

Figure 3. (a) *In situ* XRD patterns of (a1) $NaNi_{0.5}Mn_{0.5}O_2$ and (a2) $NaNi_{0.5}Sn_{0.5}O_2$ cycled between 4.2 and 2.8 V in the first cycle showing the largely delayed O3 ⇔ P3 phase transition. [63] John Wiley & Sons. [© 2018 WILEY-VCH Verlag GmbH & Co. KGaA, Weinheim]. (b) Schematic illustration shows the dual-stabilization effect (stabilization of bulk structure and interphase) of Li doping. Reprinted from [39], Copyright (2018), with permission from Elsevier.

which is beneficial for tolerating the lattice strains induced by Na^+ intercalation/deintercalation, thus mitigating the structure distortion and maintaining the original structure. Inspired by this principle, substitution of Mn^{3+} with divalent ions (e.g. Mg^{2+}, Zn^{2+}, and Cu^{2+}) has been performed. Liu *et al* investigated the effects of the substitution of Mn by Mg on the crystal structure, electronic structure, and electrochemical performances of O3–$NaMn_{0.48}Ni_{0.2}Fe_{0.3}Mg_{0.02}O_2$. Their results illustrated that a small quantity of Mg^{2+} incorporated into the structure, enlarges the Na layer spacing, which not only improves the Na^+ diffusion coefficient but also alleviates the lattice strain or the volume change, thus the irreversible phase transitions induced by sodiation/desodiation are suppressed [55]. Similar effects are also exhibited in Zn^{2+} and Cu^{2+} doped oxides. The increase in the d-layer spacing, is likely also due to the enhanced ionic bonding strength between the TM–O as discussed above. Yan and Sui conducted a comprehensive study on the degradation mechanism of layered Na_xTMO_2 oxides upon high voltage cycling by taking P2-type $Na_{2/3}Ni_{1/3}Mn_{2/3}O_2$ as an example [27]. Through systematic characterizations and statistical analysis, they found that the capacity decrease had a close correlation with the intragranular crack density, and thus determined that the phase transition induced grain cracking is the main cause of performance decay compared with surface degradation, which is different from the layered cathodes of LIBs. Yan and Sui also successfully demonstrated that intragranular cracking related degradation can be mitigated by deploying a dopant segregation strategy [72]. Based on electrochemical tests, microstructural characterizations and DFT calculation, they found that the randomly distributed Mg dopants in P2-structured $Na_{0.67}Ni_{0.33-x}Mn_{0.67}Mg_xO_2$ migrated from the TM layer and segregated into the Na layer during high-voltage cycling, which led to the formation of Mg-enriched precipitates. The electrochemical cation migration acts as 3D network pillars and enhances the material's capability to tolerate the stress caused by structural changes, suppressing cracking formation effectively during cycling. As a result, the Mg-doped electrodes showed improved cycling stability when cycled at higher charge cut-off voltage (2.0–4.5 V) with a capacity retention of 82% compared with only 67% retention cycled at 2.0–4.3 V after 100 cycles. This phenomenon can be contributed to the fewer grain cracks generated when cycled at 2.0–4.5 V than when cycled at 2.0–4.3 V. This '*in-situ*' conceptual strategy using electrochemical cation migration, opens a new direction to further engineer the bulk material and enhance high voltage cycling stability, which could be realized by adjusting cycling condition or formation protocols to control the migration in the first few cycles.

3.2.1.3. Mitigating the Jahan–Teller effect

Mn-based layered materials usually suffer from structure degradation caused by Jahan–Teller effect of Mn^{3+}. As mentioned above, the incorporation of M^{2+} cations, such as Mg^{2+}, Zn^{2+} and Cu^{2+} has been shown to effectively suppress the Jahn–Teller effect of Mn^{3+} by promoting the formation of Mn^{4+} oxidation state. This improves and reduces the phase transitions relating to the Na^+/vacancy-ordering and contributes to forming a stable structure with lower levels of sodium concentration and hence a greater reversible capacity [73].

Excess Li-ions can play a significant role in improving the capacity and modifying the surface structure of traditional layered oxides for Li-ion batteries [74] and Li-rich layered TM Na oxides have also been proposed. Kim *et al* investigated the effects of lithium substitution on sodium layered oxides [75]. A series of layered $Na_xLi_yNi_{0.25}Mn_{0.75}O_\delta$ oxides ($0.7 \leqslant x \leqslant 1.2$; $0 < y \leqslant 0.5$) were synthesized and it was observed that low levels of Li in the TM layer can act in stabilizing the crystal structure and reduce charge-ordering (superstructure) effects, in addition to the negation of Ni movement into the Na layer during cycling. As a result, the Li-substituted $Na_{0.85}Li_{0.17}Ni_{0.21}Mn_{0.64}O_2$ demonstrated a single smooth charge/discharge curve and excellent structural stability with less than 1% crystallographic volume change during cycling. Xu *et al* conducted an extensive study on the critical role of Li substitution in P2−$Na_x[Li_yNi_zMn_{1-y-z}]O_2$ ($0 < x, y, z < 1$) materials [76]. They suggested that the presence of monovalent Li^+ in the TM layer allows more Na^+ ions to remain in the prismatic sites at the end of charge to keep the overall charge balance. Consequently, the P2–O2 phase transition induced by greater Na^+ extraction was delayed up to 4.4 V vs Na/Na^+. Li-substitution has also been applied successfully to O3-type oxides with similar electrochemical observations. Meng *et al* explored the replacement effect of Li in O3 type $NaLi_xNi_{1/3-x}Mn_{1/3+x}Co_{1/3-x}O_2$ ($x = 0.07$, 0.13, and 0.2) [77]. The optimized composition, $NaLi_{0.07}Ni_{0.26}Mn_{0.4}Co_{0.26}O_2$ with single-phase, demonstrates excellent capacity retention with above 98% after 50 cycles between 1.5 V and 4.5 V vs Na/Na^+ at 125 mAg^{-1}, as well as superior rate performance when compared to non-doped. Though they attributed the improved performance to the suppressed phase transformation and enhanced electronic conductivity, the exact role of Li in stabilizing the O3 structure is still unclear. You *et al* conducted a systematic study of the potential influence of Li doping on the high-voltage electrochemistry of O3-type cathodes by taking Li-substituted $Na_{0.85}Li_{0.1}Ni_{0.175}Mn_{0.525}Fe_{0.2}O_2$ (NLNMF) as an example [39]. By using advanced experimental techniques combined with DFT theoretical calculation, they revealed that the incorporation of Li into the TM layer can suppress the unfavourable P3–P′3 phase transition at high voltage (>4.2 V versus Na^+/Na) by mitigating the Jahn–Teller distortion of Ni^{3+} during Na (de)intercalation process, thus leading to a smooth structural evolution in the bulk material during sodiation and de sodiation (only the O3–P3 phase transition was observed). In addition, this study also showed that the electrolyte-cathode interphase was effectively stabilized by introducing Li^+ ion in the TM layer. The incorporated Li^+ tends to bond with the F^- anion and coordinates with solvent molecules, which may help to prevent the unfavourable loss of active TM ions from the bulk structure, resulting in a greater stability of the CEI at high voltages (figure 3(b)). Benefiting from the dual-stabilization effect (stabilization of bulk structure and interphase), the Li-substituted NLNMF material shows improved high-voltage durability with 88% capacity retention after 100 cycles at 1 C (1 C = 150 mA g^{-1})when operated to a cut-off voltage of 4.5 V. Although its mechanism remains controversial, these Li-Na co-doped systems provide a possible feasible approach for further stabilization of the O3-type crystal structures for long-term and high voltage cycling.

Though a large number of doping elements have been reported to be effective in stabilizing the structure and improving the electrochemical performance of layered transition metal oxides, the exact role and improvement mechanism of those incorporated doping elements are still not very clear due to the difference in the size, valence, electrochemical activity, substituted atoms types, and the atoms coordination environments [55]. Although these initial results point towards dopant strategies which stabilize the structures and shift the high voltage phase transitions to lower sodium concentrations in the layered oxide (higher voltages vs Na/Na^+). This stabilization is likely achieved through changes in the ionicity of the bond strengths of the transition metal oxide layer. However, systematic research is still needed to further reveal how the introduced dopants regulate the crystal structure, and careful selection should be made according to the characteristics of the substrate and the desired improved properties.

3.2.2. Anion doping

Widening the operating voltage is undoubtedly the most direct and effective way to increase the energy density of the battery. It may, however, lead to anion redox reactions, the loss of oxygen and subsequent structural deterioration, as has been reported in both lithium and sodium battery layered materials [78–81]. Anionic doping (e.g. F^-, Cl^-, Br^-, and S^{2-}), as an effective strategy to enhance the structural stability and suppress the redox activities on oxygen anions has been studied in lithium-based layered oxides but is relatively unexplored for the sodium analogues [82–87].

Huang *et al* introduced fluorine into sodium O3-type layered oxide $NaNi_{1/3}Fe_{1/3}Mn_{1/3}O_{2-x}F_x$ for the first time to investigate the potential effects on structural and corresponding electrochemical properties [88]. They pointed out that the crystal cell parameters first decrease and then increase as a function of F^- doping, which was due to the increased proportion of Mn^{3+} (0.645 Å) rather than Mn^{4+} (0.53 Å) when O^{2-} (1.40 Å) was replaced by F^-(1.33 Å). The binding energy of TM–O enhanced with F^- doping, can help to suppress the John–Teller effect of Mn^{3+} and facilitate the Na^+ diffusion. As a result, $NaNi_{1/3}Fe_{1/3}Mn_{1/3}O_{1.99}F_{0.01}$ with the optimum F-doping level exhibited improved cycling stability and rate performance with a capacity retention of ∼90% after 70 cycles at a current density of 150 mA g^{-1}. Chen *et al* found that fluorine doping in P2-type $Na_{0.6}Mn_{0.95}Ni_{0.05}O_{2-x}F_x$ cathodes can not only stabilize the crystal structure but also boost the electrochemical reactivity of Ni^{2+}/Ni^{3+} redox couple [89]. Partial fluorine substitution in oxygen sites leads to the formation of a strong and robust Ni–F bond, which enhances the utilization of Ni^{2+}/Ni^{3+} redox couple and results in a superior reversible capacity and higher working potential. Moreover, the robust Na–F bond may prevent the collapse of the P2 phase structure with deep Na^+ deintercalation and improve its cycle stability. The doped electrode $Na_{0.6}Mn_{0.95}Ni_{0.05}O_{1.95}F_{0.05}$ showed a higher capacity of 80.76 mAh g^{-1} and capacity retention of 75.0% compared to the undoped electrode (75.49 mAh $g^{-1}$and 58.4% retention) after 960 cycles at 2 C. Recently, Liu *et al* conducted a comprehensive study on the role of F^- doping on the structural evolution and charge compensation by taking F^- substituted $Na_{2/3}Ni_{1/3}Mn_{2/3}O_{2-x}F_x$ as an example [90]. By using solid-state 19 F and 23Na NMR, XPS, EELS, and neutron diffraction, they revealed that both Ni but also Mn participate in the redox reaction process upon F^- substitution, this leads to an enhanced specific capacity of 10 mAh g^{-1}. In addition, this study also showed that F^- substitution can decrease the ordering of Ni/Mn during synthesis, which is beneficial for disrupting the John–Teller effect during cycling. Hence, the biphasic reaction induced by Jahn–Teller effect in the low voltage region was suppressed by the F^- substitution. Consequently, the F^- substituted sample delivered good cycling stability at both room temperature and high temperature of 55 °C, with a capacity retention of 94% and 75.6% after 2000 cycles at 10 C, respectively. In addition to F, B doping has also been studied. Wang *et al* introduced boron into a novel P3-type layered $Na_{0.65}Mn_{0.75}Ni_{0.25}O_2$ oxide, and found that boron doping can transform the NaMNO from P3 phase to a more stable P2 phase, as well as suppressing the oxidation-reduction of oxygen anions, thus highly stable crystal structure and remarkable cycling life are achieved [91].

Anion doping offers us an attractive way to stabilize crystal structure and enhance the cycling stability without sacrificing the specific capacity, which is a great advantage over cationic substitution. However, unlike its lithium counterpart, anion doping in sodium batteries has not been thoroughly studied. In addition to halogen elements, polyanion-type compounds $(XO_4)^{n-}$ (e.g. $SO_4{}^{2-}$ and $SiO_4{}^{4-}$) with strong covalent bonding combined with MO_x (M = transition metal) polyhedrons as doping strategies in these layered oxide could also be considered [92]. It is generally recognized that anion substitution improves the electrochemical performance by inducing a partial reduction of Mn^{4+} to Mn^{3+}, excessive Mn^{3+} will cause rapid structure degradation because of the Jahn–Teller distortion of Mn^{3+}. Thus, the anion doping amount needs to be precisely regulated to ensure this delicate balance.

3.3. Particle surface coating and modifications

In addition to the contribution from the bulk structure deterioration, the interface reactions between cathode and moisture, cathode, and electrolyte, also play vital roles in the manufacturability and determining the final performance of batteries. Surface coating, as an effective surface modification strategy, has been widely used in lithium-containing cathode materials, and various coating substances (i.e. oxides [93], fluorides [94] and phosphates [82, 95]), as well as coating methods (i.e. mechanical mixing [96], sol-gel [97], CVD [98] and ALD [99–101]) have been well developed and investigated. It is intuitively easy to apply those approaches to the development of highly stable materials for NIBs. According to the performance degradation mechanisms mentioned in section 2, the roles of surface coatings can be summarized as follows:

(a) *Reduction of insulating residues from powder surfaces.* As mentioned in section 2.2.1, most of the current oxide materials are prone to react to form carbonates and hydroxides on the surface once exposure to air, which not only forms an insulating layer upon the particle surface, but it also induces the electrode inks and slurries to gel (PVDF-NMP systems) under certain moisture and temperature conditions. Removing this layer, by forming a protective coating on the surface can prevent the active portion of the material from coming into direct contact with air in the materials storage and cathode preparation process. This in turn will facilitate easier handing of the material and make the whole manufacturing process easier with greater reproducibility. In addition, the removal of the insulating layer from the surface will benefit the cell performance; reducing the internal resistances, promoting higher capacities, higher rates and longer cycle life.

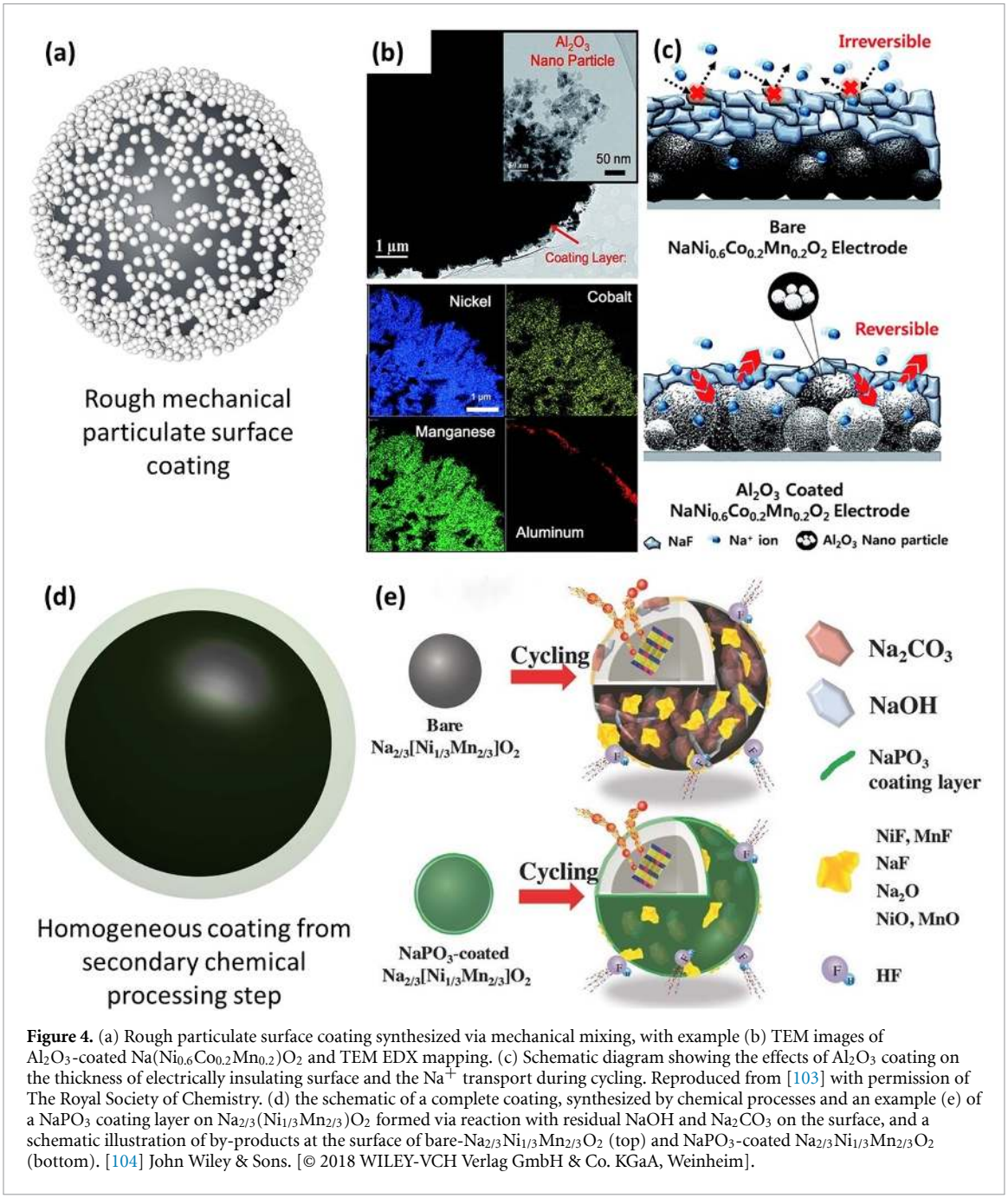

Figure 4. (a) Rough particulate surface coating synthesized via mechanical mixing, with example (b) TEM images of Al_2O_3-coated $Na(Ni_{0.6}Co_{0.2}Mn_{0.2})O_2$ and TEM EDX mapping. (c) Schematic diagram showing the effects of Al_2O_3 coating on the thickness of electrically insulating surface and the Na^+ transport during cycling. Reproduced from [103] with permission of The Royal Society of Chemistry. (d) the schematic of a complete coating, synthesized by chemical processes and an example (e) of a $NaPO_3$ coating layer on $Na_{2/3}(Ni_{1/3}Mn_{2/3})O_2$ formed via reaction with residual NaOH and Na_2CO_3 on the surface, and a schematic illustration of by-products at the surface of bare-$Na_{2/3}Ni_{1/3}Mn_{2/3}O_2$ (top) and $NaPO_3$-coated $Na_{2/3}Ni_{1/3}Mn_{2/3}O_2$ (bottom). [104] John Wiley & Sons. [© 2018 WILEY-VCH Verlag GmbH & Co. KGaA, Weinheim].

(b) *HF and H_2O scavengers.* HF is one of the by-products when $NaPF_6$ decomposes in the presence of H_2O, and it will induce the TM dissolution by attacking the cathode and dissolving its components into the electrolyte. Most of the metal oxides used for surface coating can act as HF scavenger through the following reaction: $TMO + 2HF \rightarrow TMF_2 + H_2O$. Different from the commonly used metal oxides via a self-sacrificing mechanism, recent studies have demonstrated that nano-zeolite can be used as a novel promising scavenger by trapping HF, H_2O and even CO_2 simultaneously into its open framework, which is beneficial for generating a thinner and more stable SEI layer [35, 102].

(c) *Physical protection layer.* The surface coating can also act as a barrier layer to reduce the direct contact between electrode and electrolyte, inhibiting electrolyte penetration along the grain boundary, thus suppressing the side reactions at the interface, protecting the surface from oxygen redox which occurs at high voltages and reacts with the electrolyte, as well as preventing TM dissolution.

So far, efforts have been made to investigating the effects of surface coating on the high-voltage stability for sodium layered oxide cathode, via a variety of routes. Based on the ultimate surface coating morphology, we can simply divide the surface coating into two subgroups (figure 4). (a) Mechanical coating methods to produce particulate coated rough surface coating and, (b) chemical coatings methods, where an additional step to the synthesis of the cathode is used, and a more homogeneous surface coating is produced.

3.3.1. Mechanical coating methods

Hwang *et al* have successfully modified an O3-type $Na(Ni_{0.6}Co_{0.2}Mn_{0.2})O_2$ cathode by coating Al_2O_3 nanoparticles onto the particle surface using a simple dry ball-milling route, which was carefully operated in a dry room to minimize the exposure to moisture. As expected, the coated Al_2O_3 particles effectively suppressed the parasitic reactions by scavenging HF in the electrolyte and simultaneously formed an AlF_3 protection layer on the outermost surface of particles. The reduction in HF also delayed the dissolution of transition metals, which leads to less degradation and cracking of the cathode particles (figures 4(a)–(c)) [103]. As a result, the proposed Al_2O_3-coated electrode exhibited a higher capacity of 151 mAh g^{-1}, as well as improved rate capability and capacity retention of 75% after 300 cycles in a pouch cell. A similar phenomenon was also confirmed by Liu *et al*, who enhanced the cycling stability of P2–$Na_{2/3}(Ni_{1/3}Mn_{2/3})O_2$ in the high voltage range (2.0–4.3 V) by applying a thin surface layer of Al_2O_3 [105].

Oxide coatings obtained through mechanical mixing processes possess the advantages of simplicity and low cost. However, it also demonstrates some obvious shortcomings: (a) metal oxides are generally insulating to ionic/electronic conduction. This will lead to an increase in cell polarization and reduce rate capability and cycle life. (b) Though the metal oxides can capture HF, the scavenger itself will also be constantly consumed and therefore have a finite life-time, whilst water will still be generated, further degrading the battery performance over extended period of cycling. (c) The mechanical mixing of the cathode particles with coatings is very rough, the metal oxides tend to discontinuously and incompletely cover the surface, some areas are heavily coated while other areas are only barely coated (figures 4(a)–(c)) [106]. To tackle these problems, it is necessary to develop novel coating methods and optimize the coating composition to obtain a uniform and controllable coating layer with high Na^+/e^- conductivities.

3.3.2. Chemical coating processes

Xiao *et al* successfully constructed a homogeneous layer of Na-ion conductor Na_2SiO_3 on the O3–$NaNi_{1/3}Fe_{1/3}Mn_{1/3}O_2$ electrode by an *in situ* coating approach. Firstly, a SiO_2 uniformly coated $Ni_{1/3}Mn_{1/3}Fe_{1/3}C_2O_4{\cdot}yH_2O$ was obtained by mixing $Ni_{1/3}Mn_{1/3}Fe_{1/3}C_2O_4{\cdot}xH_2O$ precursor and $Si(OC_2H_5)_4$, followed by a solvothermal process based on hydrolysis of $Si(OC_2H_5)_4$ by $Ni_{1/3}Mn_{1/3}Fe_{1/3}C_2O_4{\cdot}xH_2O$ at 180 °C. Then, $SiO_2-Ni_{1/3}Mn_{1/3}Fe_{1/3}C_2O_4{\cdot}yH_2O$ reacted with $NaCO_3$ to form Na_2SiO_3 coated $NaNi_{1/3}Fe_{1/3}Mn_{1/3}O_2$ under high-temperature calcination [107]. This coating method can not only create a uniform and complete coating layer but also forms a well adhered coating layer. The results indicate that the Na_2SiO_3 coating layer can effectively increase Na^+-ion conduction and suppress the particle cracking, whilst minimizing parasitic side reactions. Meanwhile, Na_2SiO_3 coating also effectively facilitates the reversible O3–P3 phase transitions during cycling, by preventing transition metal migration. As a result, the as-coated sample exhibits highly improved cycling stability (increased by 28% after 50 cycles) and good rate capability (58 mAh g^{-1} at a high rate of 5 C, compared to only 12 mAh g^{-1} for the pristine electrode). In a similar way, they also used 5 wt.% $Ti(OC_4H_9)_4$ to treat $Ni_{1/3}Mn_{2/3}C_2O_4{\cdot}xH_2O$ for $Na_2Ti_3O_7$-modified P2-type $Na_{2/3}Ni_{1/3}Mn_{2/3}O_2$ electrode [108].

Sodiated transition metal oxides are sensitive to moisture, NaOH and Na_2CO_3 will be immediately generated once exposed to air, resulting in Na-deficient surface with low electron and ion conductivity. There is no doubt that it would be beneficial if we could remove these sodium by-products during the coating process, simultaneously dealing with two short comings in the manufacturing process at once. Inspired by this, Myung and Sun *et al* have attempted to minimize these surface sodium residues content (Na_2O, NaOH, and Na_2CO_3) by reacting with $NH_4H_2PO_4$ via melt-impregnation at 300 °C to form a uniform coating layer on the surface of the parent $Na_{2/3}(Ni_{1/3}Mn_{2/3})O_2$ particles. During the heating process, $NH_4H_2PO_4$ spontaneously transforms to HPO_3 melt, which impregnates or encapsulates all the particles which undergoes a reaction with the surface residues to form an ionic conducting $NaPO_3$ coating layer (figures 4(d) and (e)) [104]. This artificial conformal $NaPO_3$ lowers the surface residue content but also acts as HF/H_2O scavenger to suppress the corrosion of the cathode materials (figure 4(e)), thus, structural integrity and superior cyclability are achieved. Similarly, $Ca(NO_3)_2$ and H_3PO_4 have been used to generate a uniform and ionically conducting protective layer of β-$NaCaPO_4$ on the surface of $Na_{2/3}(Ni_{1/3}Mn_{2/3})O_2$ powders after heating at 700 °C in air [109]. Like the $NaPO_3$ layer, the native β-$NaCaPO_4$ surface layer can also scavenge HF/H_2O in the electrolyte to alleviate the surface degradation phenomena. As a result, the capacity retention remarkably improved from 31% for the bare electrode to 74% for the coated electrode after 200 cycles within 2.5–4.3 V at 0.2 C. The lowering, or removal of the residual surface compounds reduce the resistances of the materials, improve ionic conductivity, and help to maintaining the integrity of the crystal structure during cycling. The removal of these surface residues is extremely important when developing these NIB oxide cathodes but is often overlooked. Future optimization strategies should include this consideration.

Surface coatings that aim to suppress surface-related chemical degradations might work in suppressing electrolyte decomposition, metal dissolution, and improving conductivity, but do not, in general, suppress

the high voltage phase transitions [32]. This is different from the layered cathodes for LIBs, where surface degradation is more dominated by bulk structure changes. The sodium-containing layered oxides possess more complicated phase transformations accompanied by repeated large volume changes during cycling. This suggests that simple coating layers, tens of nanometres in thickness, are unlikely to be robust, or flexible, enough to sufficiently compensate for the volume change and structure collapse of NIBs layered cathodes under adverse operations (high voltage and long-term cycling). Therefore, to optimize the NIBs layered oxides for high-voltage applications, the combination of bulk doping and surface coating to simultaneously stabilize the bulk structure and interface will be more effective. It should also be noted that some of the modification methods that are widely used for LIBs may not be applicable to NIBs due to the highly hygroscopic nature of sodiated transition metal oxides. Some commonly used methods that for LIB involve wet mixing and post-heating treatment which would most likely expose the layered oxides to moisture resulting in the formation of NaOH and Na_2CO_3 on the particle surfaces. Therefore, novel coating routes that minimize contact with air or liquids could be more appropriate for constructing stable particle interfaces for sodium layered oxides.

3.4. Combined composition and coating strategies

Hwang *et al* have demonstrated a combined structure modification to enhance the electrochemical performance of $Na(Ni_{0.5}Mn_{0.5})O_2$ (NM55) electrode by MgO surface coating and simultaneously doping Mg via a one-step synthesis process [110]. During the high-temperature calcination process, up to about 5 at% of Mg is uniformly incorporated into the bulk structure due to the thermodynamics (figure 5(a)), which could effectively improve the structural stability by suppressing the irreversible phase transformation. Meanwhile, the surface-related degradation process may be eliminated by the residual MgO coating layer. As a result, the co-modified NM55 cathode exhibited a significant enhanced cycling stability with 75% capacity retention after 100 cycles in the wide voltage range of 2.0–4.2 V, compared to only 46% for the bare cathode. Later, they have also applied this effective coating-induced doping strategy in O3–$Na(Ni_{0.6}Co_{0.2}Mn_{0.2})O_2$ cathode to boost the structural stability by concurrent TiO_2 coating and partial Ti doping [58]. Similarly, Xiao *et al* successfully prepared a CuO-coated and Cu^{2+}-doped co-modified P2-type $Na_{2/3}(Ni_{1/3}Mn_{2/3})O_2$ via a wet-chemistry approach [111]. The CuO covering layer hinders the corrosion of the electrolyte and prevents particle exfoliation phenomena, while the partial incorporated Cu^{2+} shrinks TMO_2 sheets and shortens TM–O bond, leading to a crystal structure with enhanced stability. The above-mentioned results suggest that the phenomenon of the coating constituents penetrating the bulk structure may be common during the annealing process, thus, a systematic study of the effect of the annealing temperature and time should be taken to elucidate the interplay between the coating and doping levels.

Guo *et al* proposed an exact opposite strategy, doping-induced surface reconstruction [41]. They found that the doped Ti^{4+} tends to concentrate on the particle surface, forming an atomic-scale interface composed of spinel-like titanium (III) oxides (figure 5(b)). This Ti(III)-concentrated spinel-like overlayer can not only suppress the atmospheric and electrochemical corrosion but also enhance the structural stability and electronic/ionic conductivity. Consequently, the Ti doping-induced surface-engineered electrode showed astonishing cycling stability with 85% capacity retention after 100 cycles at 0.5 C, compared to 36% for the Ti-free electrode. Though the underlying mechanism of this spontaneous surface segregation still needs further studies, this doping-induced surface reconstruction strategy provides new insight to tailor and modify the interface, which is completely different from the general coating methods.

Apart from the use of metal oxide as coating layer, very recently, Tang *et al* designed a dual-modified P2-type $Na_{0.67}Ni_{0.33}Mn_{0.67}O_2$ (NMO) cathode via bulk Mg substitution (NMMO) and $NaTi_2(PO_4)_3$ (NTP) surface coating through sol-gel method [112]. The bulk Mg substitution reduces the volume contraction and stabilizes the bulk structure through suppressing the P2–O2 phase transition, while the NASICON-type NTP coating layer can both stabilize the interface and facilitate the Na^+ migration due to its stable and open framework. Therefore, the dual-modified NMMO/NTP exhibited a cycling performance with 77.4% capacity retention after 200 cycles at 1 C within 2.5–4.3 V. By contrast, the bare NMO and Mg-doped NMMO electrodes showed more rapid capacity degradation, with only 19.7% and 59.8% capacity retention, respectively.

We believe that the combination of host structure doping and surface coating through *in-situ* will be supportive for achieving high energy density Na-ion batteries with improved cycling performance.

3.5. Particle morphology and material structure design

3.5.1. Multi and bi-phasic hybrid materials

As two of the most common layered oxide materials for NIBs, O3 and P2 phase oxides have been extensively investigated in the last 10 years. In general, O3 type oxides possess the advantage of a higher capacity than P2

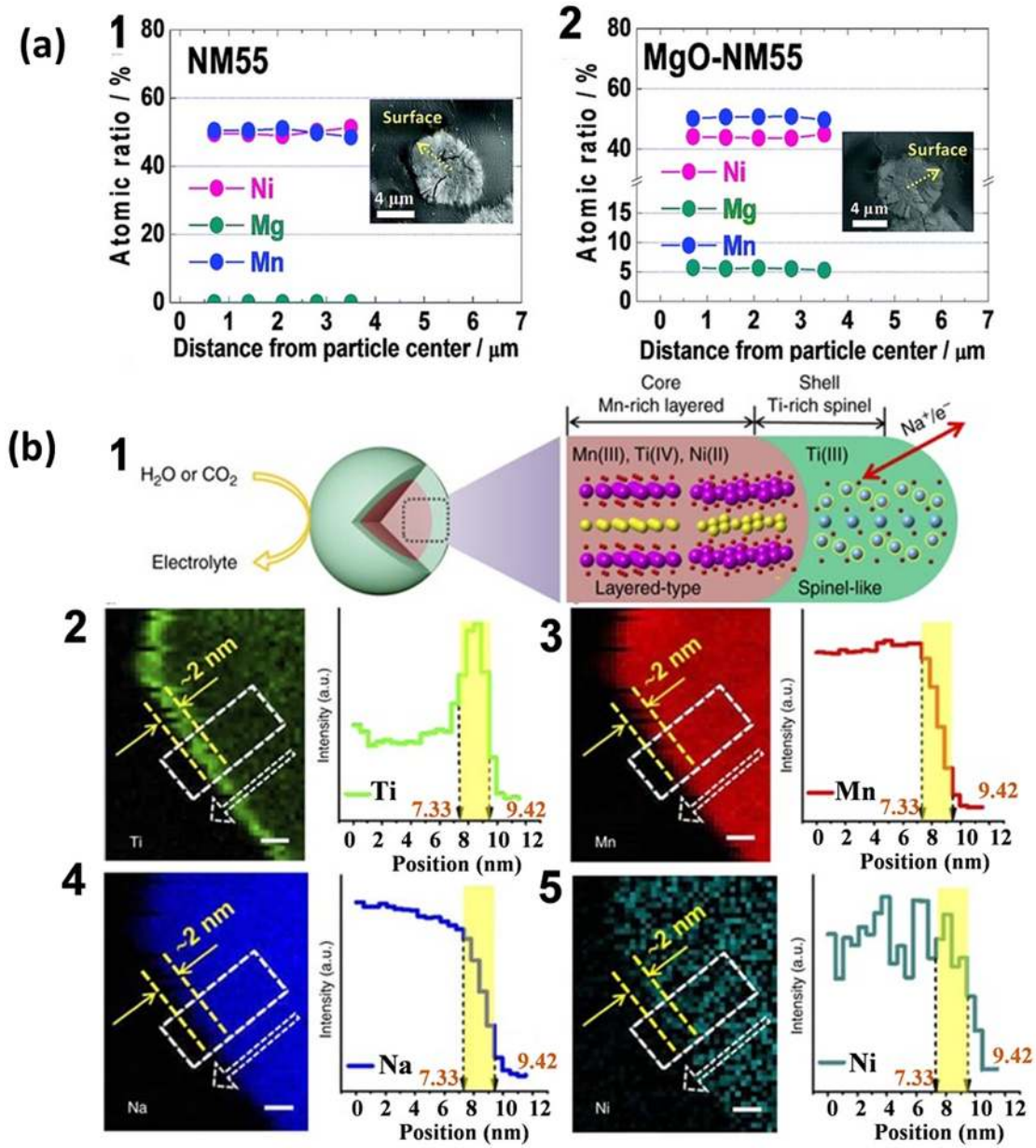

Figure 5. (a) Example of dual effect from a one-step synthesis process for fabricating the MgO coated and Mg doped $Na(Ni_{0.5}Mn_{0.5})O_2$ (MgO–NM55) cathode. EPMA results of (a1) NM55 and (a2) MgO–NM55 cathodes. Reproduced from [110] with permission of The Royal Society of Chemistry.(b1) 3D structural model of the NMTN samples composed of a Ti-rich spinel-like interface (green shell) and Mn-rich layered bulk (brown core). (b2–5) EELS chemical mapping of the NMTN samples and corresponding chemical compositions (white rectangle) for b2 Ti, b3 Na, b4 Mn, and b5 Ni elements showing that the interface 2 nm from the particle edge is enriched by titanium rather than other elements. Reproduced from [41]. CC BY 4.0.

type but suffer from unsatisfactory cycling properties owing to the easily contaminated surface and complex phase transitions during the electrochemical process. P2 type oxides are just the opposite, these oxides possess relatively strong resistances to hygroscopic degradation, and can maintain its original structure over a wider voltage range, thus exhibiting improved capacity retention. However, the lower capacity and an initial coulombic efficiency higher than 100%, as observed in a sodium metal anode cell. This efficiency originates from the deficient sodium content and the further electrochemical sodiation of the material upon discharge. This not only narrows its competitiveness in terms of energy density but brings many difficulties in terms of the full cell design. Though efforts have been devoted to modifying the structure and overcome the intrinsic drawbacks of each material, it is still a challenge to obtain an ideal cathode material which possesses all the desired properties, namely high capacity, robust structure, as well as superior rate capability. Therefore, hybrid material structures have been designed with biphasic O3 and P2 phases to combine the merits and offset the drawbacks of the two pure phases, and a series of composite cathodes with biphasic O3/P2 phases have been proposed.

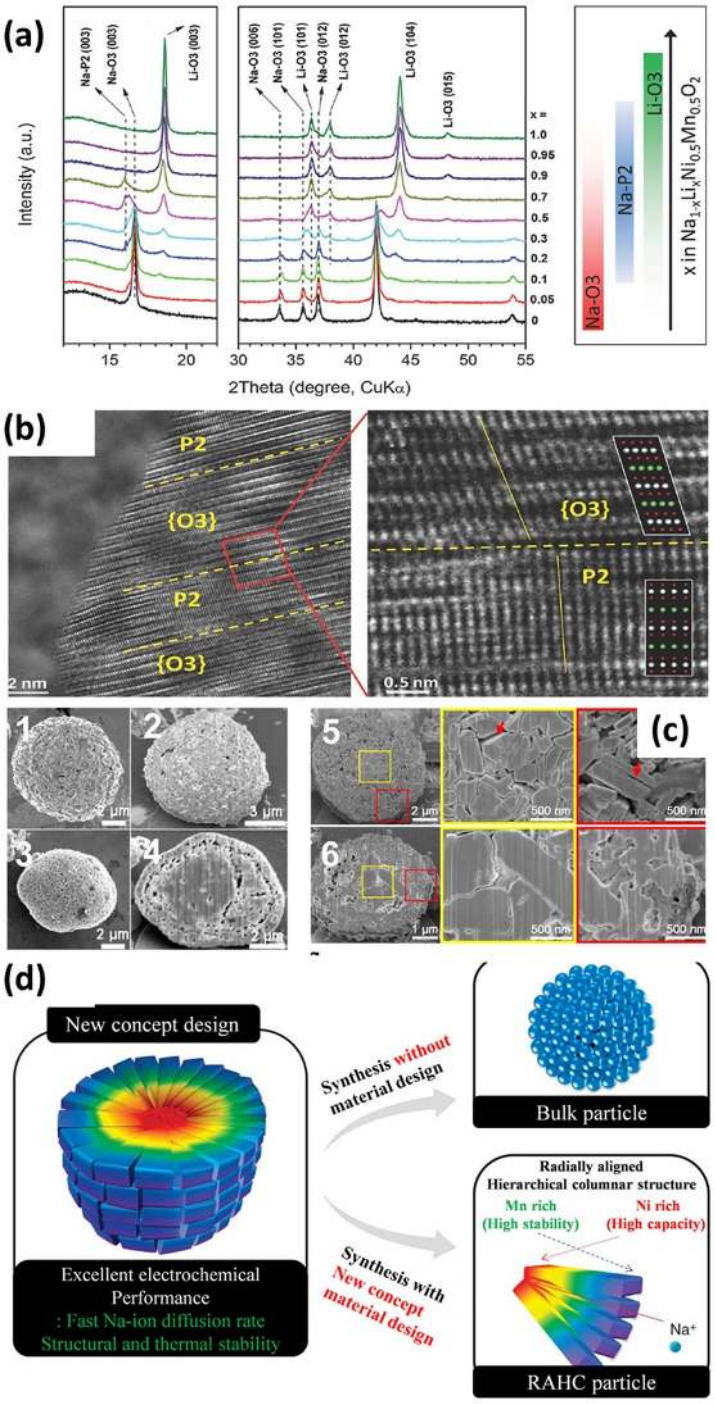

Figure 6. (a) X-ray diffraction patterns of $Na_{1-x}Li_xNi_{0.5}Mn_{0.5}O_{2+d}$ with different Li content, x ($0 \leq x \leq 1$) showing phase evolution of $Na_{1-x}Li_xNi_{0.5}Mn_{0.5}O_{2+d}$ as a function of Li content. (b) High-resolution TEM images directly showing the intergrowth stacking of the P2 and O3 lattices of $Na_{0.7}Li_{0.3}Ni_{0.5}Mn_{0.5}O_{2+d}$. [113] John Wiley & Sons. [© 2014 WILEY-VCH Verlag GmbH & Co. KGaA, Weinheim]. (c1, c2) Representative plan-view and cross-sectional SEM images of the pristine O3/O′3 material. (c3, c4) Representative plan-view and cross-sectional SEM images of the pristine O3/O′3–P2 material. Comparison of cross-sectional SEM image of the (c5) pristine O3/O′3 and the (c6) O3/O′3–P2 electrode after 50 cycles. Reprinted with permission from [114]. Copyright (2020) American Chemical Society. (d) Scheme illustration of the composition and structure for a typical RAHC particle. Reprinted by permission from Springer Nature Customer Service Centre GmbH: [Nature] [Nature Communications] [115] (2015).

Johnson *et al* first reported layered O3/P2 intergrowth cathode in the study of the effects of Li substitution for Na in $Na_{1-x}Li_xNi_{0.5}Mn_{0.5}O_2$ [113]. They found that with Li substitution, the P2 phase fraction increases at the expense of O3 until $x = 0.5$ (figures 6(a) and (b)), and the capacity, as well as rate capability significantly improved simultaneously. However, due to the dominant quantity of the O3 phase in this hybrid material, the O3–P3 phase transition is still inevitable. This exhibits a disadvantage, resulting in a significant decrease in capacity within 20 cycles. Based on this, Zhou *et al* proposed an opposite design strategy, namely introducing minor O3 phases into the P2 host material to increase the capacity while

ensuring good cycling performance and rate capability [116]. The synthesized P2-majority composite material $Na_{0.66}Li_{0.18}Mn_{0.71}Ni_{0.21}Co_{0.08}O_2$ presented an improved capacity of 200 mAh g^{-1} (compared with 125 mAh g^{-1} of corresponding single P2), rate capability, cycling stability in the wide voltage range of 1.5–4.5 V (75% capacity retention over 150 cycles) and higher average voltage of 3.2 V vs Na/Na^+. This average voltage and capacity give a gravimetric energy density of 640 Wh kg^{-1} which rivals that of $LiFePO_4$ (about 530 Wh kg^{-1}).

In addition to the Li substitution for Na mentioned above, Li substitution for TMs has also been proven a feasible strategy for synthesis of bi-phasic materials. Liu *et al* have successfully obtained P2/O3 biphasic $Na_{0.67}Mn_{0.55}Ni_{0.25}Ti_{0.2-x}Li_xO_2$ by Li substitution for Ti [117]. XRD refinement showed that the O3-phase content increases from 0% to 14.87% for $x = 0$–0.2. The Li mainly occupies the TM sites, maintaining the P2 structure, while a low level of Li resides in the Na sites to adjust the Na/TM ratio required for the O3-phase. The generation of the O3 phase improves the observed Na ion diffusion kinetics, this improvement may originate from the greater number of defects with the lower valence of Li^+ compared to $Ti4^+$. Similarly, the work of Huang *et al* showed that Mg can also be used to substitute TM in layered $Na_{0.67}(Fe_{0.5}Mn_{0.5})_{1-x}Mg_xO_2$ to obtain a P2/O3 bi-phasic cathode $Na_{0.67}Fe_{0.425}Mn_{0.425}Mg_{0.15}O_2$, which can deliver 155 mAh g^{-1} and good cycling stability within 2.0–4.3 V [118].

Chen *et al* synthesized a series of O3/P2 hybrid cathodes with various O3/P2 ratio by adjusting the sodium content in $Na_xNi_{0.2}Fe_{x-0.4}Mn_{1.2-x}O_2$ [119]. Structural refinements showed that the sodium content $x = 0.8$ is a critical value, above which the pure O3 phase formed, while below 0.8 a O3/P2 hybrid structure is obtained. The optimized formula $Na_{0.78}Ni_{0.2}Fe_{0.38}Mn_{0.42}O_2$ displays the best comprehensive electrochemical performance in terms of capacity, rate capability, and cycling stability. Notably, superior cycling performance was obtained with 90% capacity retention after 1500 cycles within 2.5–4.0 V. This suggests that the high voltage phase transition was not observed within the voltage limits utilized in this study. Further doping strategies could improve the observed specific capacities with increased cycling voltage windows, increasing the observed average voltage whilst maintaining the cycle life.

Apart from P2/O3 hybrid structure, other intergrowth systems, such as P2/P3 [120–122], P2/tunnel [73, 123], and some multiphasic intergrowth materials (O3/P2/P3 or P2/O3/O1) [124, 136] have also been proposed and studied.

Multi-phasic materials combine the advantages of different phases and provide a new avenue for exploring novel cathodes with superior comprehensive performance. However, the exact interplay mechanism of different phases has not yet been fully discussed and understood, and it is still a big challenge to synthesize a multiphase cathode material with the correct desirable phase composition due to the complex and uncertain synthesis parameters [125, 136]. In addition, whilst these materials have some advantages, bi and multi-phase materials may also have some negative effects, such as extremely complex electrochemical redox reactions, and consequently complex charge and discharge voltage curves. This may pose greater challenges for state of charge management and prediction in practical applications. Therefore, it is necessary to optimize the ratio between O3 and P2 phases within a specific system to achieve a balance between electrochemical properties and the difficulty of translation into practical applications.

3.5.2. Core–shell particles

As mentioned above, designing composite phase bulk materials integrate the advantages of separate phases, and demonstrate a positive cooperative effect on the overall performance through suppressing irreversible bulk phase transitions or providing additional capacity. This approach still leaves the surface-associated chemical degradation un-solved with open facets and surfaces exposed to the electrolyte, which may enable further parasitic reactions to occur.

Considering this, a novel core–shell structure was proposed by Chen *et al* with Ni-rich O3/O′3 phases $Na_{0.8}(Ni_{0.5}Co_{0.2}Mn_{0.3})O_2$ as the core and a Mn-rich P2 phase $Na_{0.8}(Ni_{0.33}Mn_{0.67})O_2$ as the shell. This was synthesized by a two-step co-precipitation method [114]. Complementary microscopy analysis indicated that both the microscale core–shell and nanoscale internal crystal structure interfaces are well formed. The thick and continuous P2 shell appeared robust enough to constrain the structural degradation and crack propagation of the O3-type core, but also provided a stable interface by blocking the chemical attack from the electrolyte (figure 6(c)). Moreover, the incorporation of a redox active and stable phase, in this case, P2 oxide, means that the shell can participate in the electrochemistry process and facilitate the Na ions diffusion, in addition to the main core. Thus, improved cycling performance, higher reversible capacity, and improved rate capability compared to the bare O3/O′3 cathode was observed.

This core–shell architecture method uses cathode materials with electrochemically active and stable structures as coating substances without sacrificing the capacity. Hence, core–shell structure has been widely used and researched in developing superior cathode materials for LIBs [126–129], and even applied in other types of positive electrode materials for NIBs, such as polyanionic compounds [130, 131], and Prussian blue

analogues [132–135]. There is significant scope for further exploring this method for new higher energy density and stable sodium layered oxides for NIBs.

3.5.3. Concentration gradient particles

Though the core–shell configuration integrates the advantages of surface coating and hybrid bulk structures, the structure mismatch issue between the core and the shell should be carefully considered when designing this heterostructure. For example, when charged up to 4.0 V, the O3 type core materials transfer to P3 phase with large expansion in d-spacing, while the P2 type shell materials can maintain its original structure before being charged to 4.2 V [114]. This large difference in volume change between the two types of materials during Na insertion/extraction can lead to large voids at the core/shell interface upon cycling, which may result in poor connections between the core and shell, which will inhibit the transfer of Na^+ and electrons, and lead to a sudden drop in capacity from the increased resistance and poor transport properties.

To tackle this issue, a full concentration gradient (FCG) strategy was proposed by Sun *et al* for high-energy LIB cathode materials. They created a special structure where the concentration of elements providing high capacity (usually Ni or Co) decreases linearly, whereas the concentration of elements improving the structure stability (usually Mn or Al) increases linearly from the centre to the outer layer of each particle, forming a special 'core-shell' structure with Ni-rich core and Mn-rich shell [137]. Unlike the core–shell structure, this FCG structure has no obvious interface, owing to the continuous and smooth transition of components from the bulk to the surface. Consequently, the structure mismatch caused by the sharp differentiation of components in the core and shell can be effectively alleviated.

This strategy was further applied to sodium-containing cathode materials. A full concentration gradient for sodium O3-type layered oxide was reported whose chemical composition varied from the inner end ($Na[Ni_{0.75}Co_{0.02}Mn_{0.23}]O_2$) to the outer end ($Na[Ni_{0.58}Co_{0.06}Mn_{0.36}]O_2$), giving an average chemical composition of $Na(Ni_{0.6}Co_{0.05}Mn_{0.35})O_2$ (figure 6(d)) [115]. This material presented a so-called radially aligned hierarchical columnar structure (RAHC), which is different from the traditional spherical stacking structure. The hierarchical columnar structure provides extended fast channels for Na^+ ion diffusion and was also found to a greater level of Ni^{3+} rather than Ni^{2+}, which has a lower energy level of Ni^{3+}/Ni^{4+} than Ni^{2+}/Ni^{3+} redox reaction. This was reported the reasoning behind the improved discharge capacity (157 mAh g^{-1}) for the RAHC $Na(Ni_{0.6}Co_{0.05}Mn_{0.35})O_2$ at 15 mA g^{-1}, compared to the standard homogeneous bulk material; $Na(Ni_{0.6}Co_{0.05}Mn_{0.35})O_2$ (145 mAh g^{-1}), despite having identical chemical compositions. In addition, these rod-shaped primary particles showed smaller surface area and pore volume values, this minimizes the side reactions with the electrolyte, and improved cycling stability. 300 cycles were achieved in full cell with hard carbon as anode (RAHC: 80.0%, bulk: 49.2%). Moreover, the RAHC electrode, when charged to 4.1 V exhibited lower heat generation of 172 J g^{-1} at a higher temperature (293.5 °C) compared to the conventional material (321.6 J g^{-1} at 266.5 °C) when heated with electrolyte. This indicates that the thermal runaway temperature onset may be increased, and that the surface is stabilized to reaction with the electrolyte. This may be due to the reduction in catalytic sites from increased manganese content at the surface or that the RAHC structure reduces the oxygen evolution from the host structure by increasing the observed voltage at which the irreversible phase transformation occurs. By taking advantages of the concentration gradients of the transition metals and radially aligned columnar structure, high capacity and cycling performance as well as thermal stability were simultaneously achieved.

This chemistry and particle structure offers routes for stable high energy density cathode materials for NIBs without sacrificing the cycling stability. However, the synthesis of FCG materials requires a multistep co-precipitation process, which usually requires additional tanks to hold and precisely regulate the feeding rate of transition metals, increasing the time and capital cost.

Recently, a novel simplified one-step co-precipitation method for Li-based FCG cathode was proposed by using polystyrene beads as a sacrificial template [138]. This and other templating methods could provide alternative routes to particle structure manipulation, for highly stable NIB layered oxide cathodes.

3.6. Morphology and particle engineering

As mentioned in section 2.1, the excessive deintercalation of sodium ions at high voltages will involve detrimental multi-phase transitions, accompanied by large crystal unit cell volumes changes. The repeated expansion and contraction of the crystal lattice causes high strain in phase boundaries and within particles due to the difference in these lattice parameters, which can further lead to the formation of intergranular cracks between primary particles within the secondary agglomerated particles. This expansion mechanism destroys the contact between primary particles, reducing the number of electronic and ionic transport paths within the cathode particle. The consequence is high observed resistances, which subsequently leads to degradation in the cycling performance, poor rate, and occasionally lower observed capacities if the particles are completely isolated.

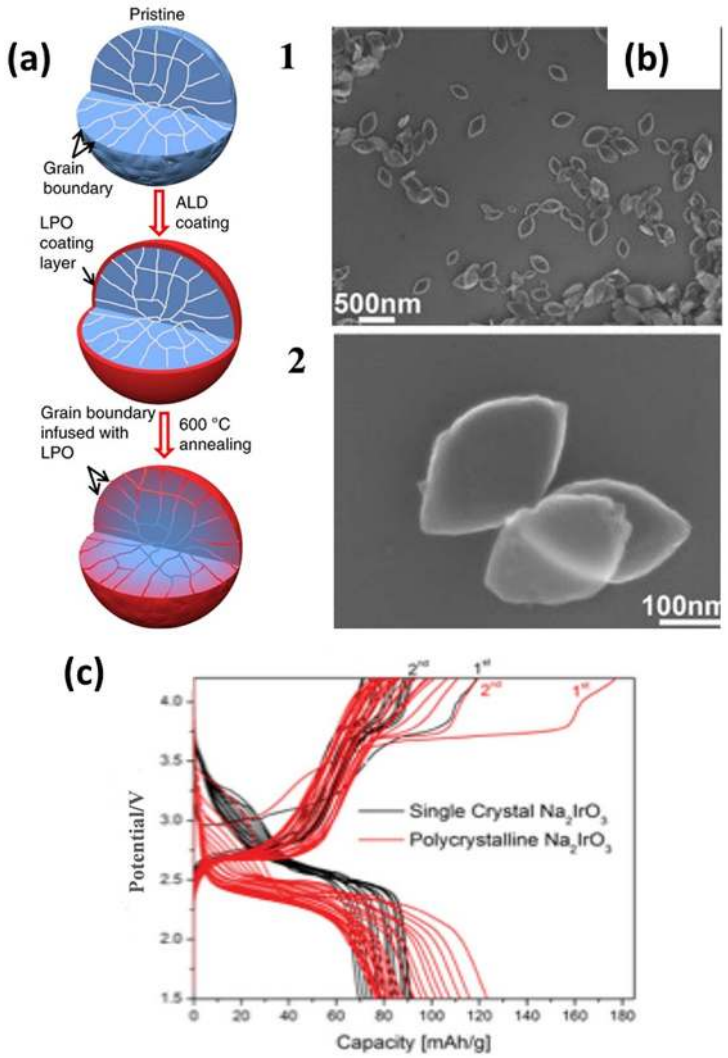

Figure 7. (a) Schematic illustration shows the evolution of the Li_3PO_4 coating layer on the secondary particle following coating and annealing. Reprinted by permission from Springer Nature Customer Service Centre GmbH: [Nature] [Nature Energy] [143] (2018). (b1) Low- and (b2) high-magnification FESEM images of $Na_{0.7}MnO_2$ nanoplates. [145] John Wiley & Sons. [© 2013 WILEY-VCH Verlag GmbH & Co. KGaA, Weinheim]. (c) Capacity–voltage plots of the very first 20 cycles obtained from a single-crystal and polycrystalline Na_2IrO_3 electrodes in the voltage window 1.5–4.2 V. [144] John Wiley & Sons. [© 2020 WILEY-VCH Verlag GmbH & Co. KGaA, Weinheim].

There are several conceptual strategies to tackle this expansion and cracking problem at a particle level rather, in addition to those discussed above, including grain boundary engineering and single crystal particles.

3.6.1. Grain boundary engineering

Grain boundary engineering is a classic and powerful approach to tailor grain boundary structure and chemistry for the optimization of material properties in material science [139–142]. However, it has not attracted enough attention in the field of batteries, e.g. lithium-ion or sodium-ion batteries. In 2018, Yan *et al* used this strategy to develop Ni-rich layered cathodes LIBs, and systematically studied its effects on structure and electrochemical properties [143]. They infused the grain boundaries of secondary particles with a solid electrolyte (Li_3PO_4) through surface coating and subsequent annealing treatment at 600 °C (figure 7(a)). Detailed structural and chemical analysis revealed that the grain-boundary modification played a vital role in enhancing the structural stability and electrochemical properties. The grain boundaries provided additional transport paths for lithium-ion conduction but also act as a blocking agent for preventing the penetration of liquid electrolyte into the boundaries, thus successfully eliminating the interfacial reactions, and suppressing the cracking of secondary particles. Although grain boundary engineering has demonstrated its effectiveness in alleviating the degradation associated with intergranular cracks in layered lithium transition cathodes [144]. However, it is yet to be applied to sodium-ion cathodes and is a promising area for future NIB cathode particle morphology and compositional optimization.

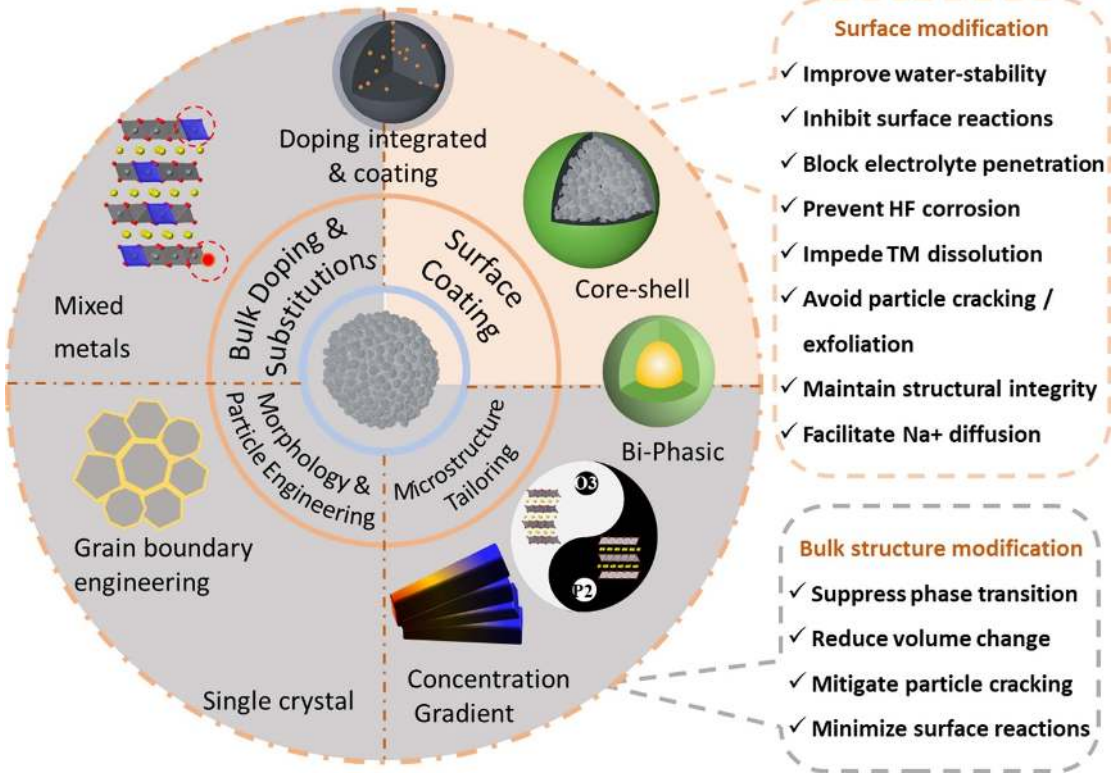

Figure 8. Overview on corresponding modifying strategies for sodium layered oxide materials under high voltage operation.

3.6.2. Single crystal particles

Single crystalline particles formed by adjusting sintering temperature and alkali/transition metal molarity offers another strategy for mitigating the issues cause because of cracks forming between primary particles.

Single crystal lithium-based cathodes, like NMC532, NMC622, NCA, were shown to demonstrate superior stability at high voltages compared to conventional polycrystalline particles [144]. It is expected that single crystal sodium-based layered oxides could also provide structural stability and improved electrochemical properties compared to typical polycrystalline materials. In 2013, Wang *et al* successfully synthesized single crystalline rhombus-shaped $Na_{0.7}MnO_2$ nanoplates by a hydrothermal method (figure 7(b)). Electrochemical tests showed that the single crystalline $Na_{0.7}MnO_2$ exhibited a near theoretical capacity of 164 mAh g^{-1}, a good high-rate performance, and a durable cyclability [145]. Tepavcevic *et al* reported a highly ordered single crystal Na_2IrO_3 electrode that may boost the energy density of NIBs [144]. Compared to its polycrystalline counterpart, single crystal Na_2IrO_3 electrode presented an improved cycling stability in the voltage window 1.5–4.2 V (figure 7(c)). Though the single crystal Na_2IrO_3 still experienced strong capacity fade with cycling because of the formation of a new phase, this single crystal strategy can play a vital role in understanding and developing novel new cathodes with robust structure.

4. Conclusions and critical opinions

In summary, NIBs offer a wealth of possibilities for the development of inexpensive and sustainable energy storage devices. However, many challenges are inevitably encountered in the pursuit of higher energy density to make it a true 'drop-in' technology for LIBs. In this review, the main aspects of degradation at high-voltage sodium layered oxide type materials are summarized:

(a) *Reactive surfaces*: the oxides are prone to react with water and CO_2 to form NaOH and Na_2CO_3 on the particle surface, which will induce possible ink gelation during the mixing and coating procedures, increase the cell polarization, as well as cause water formation from reacting with the electrolyte in a cell.

(b) *Electrolyte oxidation and oxygen loss*: high voltage operation often involves partial oxygen redox, which will result in the decomposition of electrolyte via oxidation reaction.

(c) *Surface reconstruction*: with the loss of oxygen, transition metals are reduced, and ultimately resulting in metals dissolution into electrolyte (particularly Mn^{3+}) and surface reconstruction. These dissolved transition metal ions then deposit on the anode to form a resistive interface.

(d) *Phase transitions and induced particle cracking*: the large volume change during complex phase transformations along with the enhancement of the degradation surface effects can induce cracking and pulverizing of the particles. The cracks within the particles will further lead to poor electronic conduction, TM dissolution, surface corrosion, and electrolyte consumption.

To prevent the above degradation mechanisms, various strategies including bulk-doping, surface coating, microstructure tailoring, and particle morphology design, have been investigated to date (figure 8). However, it should be noted that the bulk structure and surface degradations do not occur independently but work synergistically leading to the cathode failure at high voltages. Thus, a single approach is unlikely to eliminate all the degradation issues. We believe that to develop sodium layered oxide materials with simultaneous high energy density and long cycle life a multi-approach is required. In particular, the morphological control of the particles to produce materials with few grain boundaries or single crystals is of great importance to minimize the surface side reactions and reduce cracking along the grain boundaries thus limiting any surface-related degradations. Meanwhile, constructing a stable interface to generate residual-free particle surfaces will be beneficial for improving the manufacturability, and the stability in the cell. In addition, the voltage or average voltage needs to be increased through elective element substitution to stabilize the 'high voltage region' (associated with the oxygen redox and loss), thus minimizing the irreversible phase transitions at higher voltages, and maximizing the solid solution zone. Furthermore, HF and H_2O scavengers are required to limit the formation of fluorides on the surface of the cathodes. Therefore, constructing a synergetic structure through particle morphology design, bulk doping and surface coating is proposed to simultaneously reduce the irreversible phase transformation and surface degradation.

In addition to enhancing the stability of cathode materials itself, more attention should be focused on interfacial engineering by developing new electrolytes with wider electrochemical stability window and optimizing the formation process to form a dense, stable, and high ionic conductivity CEI film on the cathode/electrolyte surface.

Data availability statement

No new data were created or analysed in this study.

Acknowledgments

The University of Birmingham is thanked for providing doctoral funding, and Ethan Williams and David Burnett are acknowledged for their proof-reading support.

ORCID iD

Emma Kendrick https://orcid.org/0000-0002-4219-964X

References

[1] Armand M and Tarascon J-M 2008 *Nat. Commun.* **451** 652–7
[2] Cheng F, Liang J, Tao Z and Chen J 2011 *Adv. Mater.* **23** 1695–715
[3] Liu Q, Hu Z, Chen M, Zou C, Jin H, Wang S, Chou S-L and Dou S-X 2019 *Small* **15** 1805381
[4] Wang P-F, You Y, Yin Y-X and Guo Y-G 2018 *Adv. Energy Mater.* **8** 1701912
[5] Roberts S and Kendrick E 2018 *Nanotechnol. Sci. Appl.* **11** 23–33
[6] Sun Y, Guo S and Zhou H 2019 *Energy Environ. Sci.* **12** 825–40
[7] Han M H, Gonzalo E, Singh G and Rojo T 2015 *Energy Environ. Sci.* **8** 81–102
[8] Yang X, Liang H-J, Yu H-Y, Wang M-Y, Zhao X-X, Wang X-T and Wu X-L 2020 *J. Phys. Mater.* **3** 042004
[9] Kubota K and Komaba S 2015 *J. Electrochem. Soc.* **162** A2538
[10] Hwang J Y, Myung S T and Sun Y K 2017 *Chem. Soc. Rev.* **46** 3529–614
[11] Li W-J *et al* 2017 *Adv. Energy Mater.* **7** 1700274
[12] Liu T *et al* 2019 *Energy Environ. Sci.* **12** 1512–33
[13] Vassilaras P, Ma X, Li X and Ceder G 2012 *J. Electrochem. Soc.* **160** A207–11
[14] Han M H, Gonzalo E, Casas-Cabanas M and Rojo T 2014 *J. Power Sources* **258** 266–71
[15] Wang L, Wang J, Zhang X, Ren Y, Zuo P, Yin G and Wang J 2017 *Nano Energy* **34** 215–23
[16] Wang P F, You Y, Yin Y X, Wang Y S, Wan L J, Gu L and Guo Y G 2016 *Angew. Chem., Int. Ed.* **55** 7445
[17] Wang H, Yang B, Liao X-Z, Xu J, Yang D, He Y-S and Ma Z-F 2013 *Electrochim. Acta* **113** 200–4
[18] Yabuuchi N, Kajiyama M, Iwatate J, Nishikawa H, Hitomi S, Okuyama R, Usui R, Yamada Y and Komaba S 2012 *Nat. Mater.* **11** 512–7
[19] Pahari D and Puravankara S 2020 *J. Power Sources* **455** 227957
[20] Lee D H, Xu J and Meng Y S 2013 *Phys. Chem. Chem. Phys.* **15** 3304–12
[21] Mariyappan S, Wang Q and Tarascon J M 2018 *J. Electrochem. Soc.* **165** A3714–22
[22] Komaba S, Yabuuchi N, Nakayama T, Ogata A, Ishikawa T and Nakai I 2012 *Inorg. Chem.* **51** 6211–20

[23] Ding F *et al* 2020 *Energy Storage Mater.* **30** 420–30
[24] Mariyappan S, Marchandier T, Rabuel F, Iadecola A, Rousse G, Morozov A V, Abakumov A M and Tarascon J-M 2020 *Chem. Mater.* **32** 1657–66
[25] Sathiya M, Hemalatha K, Ramesha K, Tarascon J M and Prakash A S 2012 *Chem. Mater.* **24** 1846–53
[26] Xiao Y *et al* 2020 *Adv. Funct. Mater.* **30** 2001334
[27] Wang K, Yan P and Sui M 2018 *Nano Energy* **54** 148–55
[28] Xie Y *et al* 2016 *Adv. Energy Mater.* **6** 1601306
[29] Jeong M, Lee H, Yoon J and Yoon W S 2019 *J. Power Sources* **439** 227064
[30] Buchholz D, Chagas L G, Vaalma C, Wu L and Passerini S 2014 *J. Mater. Chem.* A **2** 13415–21
[31] Duffort V, Talaie E, Black R and Nazar L F 2015 *Chem. Mater.* **27** 2515–24
[32] Xiao B and Sun X 2018 *Adv. Energy Mater.* **8** 1802057
[33] Han M H, Sharma N, Gonzalo E, Pramudita J C, Brand H E A, López Del Amo J M and Rojo T 2016 *J. Mater. Chem.* A **4** 18963–75
[34] Zhang Y, Zhang R and Huang Y 2019 *Front. Chem.* **7** 335
[35] Chen L, Kishore B, Walker M, Dancer C and Kendrick E 2020 *Chem. Commun.* **56** 11609–12
[36] Alvarado J, Ma C, Wang S, Nguyen K, Kodur M and Meng Y S 2017 *ACS Appl. Mater. Interfaces* **9** 26518–30
[37] Wohlfahrt-Mehrens M, Vogler C and Garche J 2004 *J. Power Sources* **127** 58–64
[38] Zheng H, Sun Q, Liu G, Song X and Battaglia V S 2012 *J. Power Sources* **207** 134–40
[39] You Y, Xin S, Asl H Y, Li W, Wang P F, Guo Y G and Manthiram A 2018 *Chemistry* **4** 2124–39
[40] You Y and Manthiram A 2018 *Adv. Energy Mater.* **8** 1701785
[41] Guo S, Li Q, Liu P, Chen M and Zhou H 2017 *Nat. Commun.* **8** 135
[42] Mu L *et al* 2018 *Adv. Energy Mater.* **8** 18101975
[43] Song X, Meng T, Deng Y, Gao A, Nan J, Shu D and Yi F 2018 *Electrochim. Acta* **281** 370–7
[44] Wang Y, Xiao R, Hu Y S, Avdeev M and Chen L 2015 *Nat. Commun.* **6** 6954
[45] Toumar A J, Ong S P, Richards W D, Dacek S and Ceder G 2015 *Phys. Rev. Appl.* **4** 064002
[46] Wang P F, Yao H R, Liu X Y, Yin Y X, Zhang J N, Wen Y, Yu X, Gu L and Guo Y-G 2018 *Sci. Adv.* **4** eaar6018
[47] Gutierrez A, Dose W M, Borkiewicz O, Guo F, Avdeev M, Kim S, Fister T T, Ren Y, Bareño J and Johnson C S 2018 *J. Phys. Chem.* C **122** 23251–60
[48] Kang S M, Park J H, Jin A, Jung Y H, Mun J and Sung Y E 2018 *ACS Appl. Mater. Interfaces* **10** 3562–70
[49] Tie D, Gao G, Xia F, Yue R, Wang Q, Qi R, Wang B and Zhao Y 2019 *ACS Appl. Mater. Interfaces* **11** 6978–85
[50] Wu X, Xu G L, Zhong G, Gong Z, McDonald M J, Zheng S, Fu R, Chen Z, Amine K and Yang Y 2016 *ACS Appl. Mater. Interfaces* **8** 22227–37
[51] Chen T, Guo J, Zhuo Y, Hu H, Liu W, Liu F, Liu P, Yan J and Liu K 2019 *Energy Storage Mater.* **20** 263–8
[52] Deng J, Luo W-B, Lu X, Yao Q, Wang Z, Liu H-K, Zhou H and Dou S-X 2018 *Adv. Energy Mater.* **8** 1701610
[53] Rahman M M *et al* 2018 *Energy Environ. Sci.* **11** 2496–508
[54] Wang Q, Mariyappan S, Vergnet J, Abakumov A M, Rousse G, Rabuel F, Chakir M and Tarascon J-M 2019 *Adv. Energy Mater.* **9** 1901785
[55] Zhang C, Gao R, Zheng L, Hao Y and Liu X 2018 *ACS Appl. Mater. Interfaces* **10** 10819–27
[56] Yao H-R, Wang P-F, Wang Y, Yu X, Yin Y-X and Guo Y-G 2017 *Adv. Energy Mater.* **7** 1700189
[57] Sun X, Jin Y, Zhang C-Y, Wen J-W, Shao Y, Zang Y and Chen C-H 2014 *J. Mater. Chem.* A **2** 17268–71
[58] Yu T-Y, Hwang J-Y, Bae I T, Jung H-G and Sun Y-K 2019 *J. Power Sources* **422** 1–8
[59] Hwang T, Lee J H, Choi S H, Oh R G, Kim D, Cho M, Cho W and Park M-S 2019 *ACS Appl. Mater. Interfaces* **11** 30894–901
[60] Leng M, Bi J, Wang W, Xing Z, Yan W, Gao X, Wang J and Liu R 2020 *J. Alloys Compd.* **816** 152581
[61] Zhao Y, Xia M, Hu X, Zhao Z, Wang Y and Lv Z 2015 *Electrochim. Acta* **174** 1167–74
[62] Wang P F, Xin H, Zuo T T, Li Q, Yang X, Yin Y X, Gao X, Yu X and Guo Y-G 2018 *Angew. Chem., Int. Ed. Engl.* **57** 8178–83
[63] Sathiya M, Jacquet Q, Doublet M-L, Karakulina O M, Hadermann J and Tarascon J-M 2018 *Adv. Energy Mater.* **8** 1702599
[64] Rong X *et al* 2019 *J. Energy Chem.* **31** 132–7
[65] Rong X, Gao F, Ding F, Lu Y, Yang K, Li H, Huang X, Chen L and Hu Y-S 2019 *J. Mater. Sci. Technol.* **35** 1250–4
[66] Li J *et al* 2020 *J. Power Sources* **449** 227554
[67] Tripathi A, Rudola A, Gajjela S R, Xi S and Balaya P 2019 *J. Mater. Chem.* A **7** 25944–60
[68] Meng Y, An J, Chen L, Chen G, Shi L, Lu M and Zhang D 2020 *Chem. Commun.* **56** 8079–82
[69] Mao Q, Zhang C, Yang W, Yang J, Sun L, Hao Y and Liu X 2019 *J. Alloys Compd.* **794** 509–17
[70] Sun L *et al* 2018 *Small* **14** e1704523
[71] Zhang K *et al* 2019 *Nat. Commun.* **10** 5203
[72] Wang K, Wan H, Yan P, Chen X, Fu J, Liu Z, Deng H, Gao F and Sui M 2019 *Adv. Mater.* **31** 1904816
[73] Chen T R *et al* 2018 *ACS Appl. Mater. Interfaces* **10** 10147–56
[74] Xu B, Fell C R, Chi M and Meng Y S 2011 *Energy Environ. Sci.* **4** 2223–33
[75] Kim D, Kang S-H, Slater M, Rood S, Vaughey J T, Karan N, Balasubramanian M and Johnson C S 2011 *Adv. Energy Mater.* **1** 333–6
[76] Xu J, Lee D H, Clément R J, Yu X, Leskes M, Pell A J, Pintacuda G, Yang X-Q, Grey C P and Meng Y S 2014 *Chem. Mater.* **26** 1260–9
[77] Xu J, Liu H and Meng Y S 2015 *Electrochem. Commun.* **60** 13–6
[78] Du K, Zhu J, Hu G, Gao H, Li Y and Goodenough J B 2016 *Energy Environ. Sci.* **9** 2575–7
[79] Rong X *et al* 2019 *Joule* **3** 503–17
[80] Zhao C, Wang Q, Lu Y, Hu Y-S, Li B and Chen L 2017 *J. Phys. D: Appl. Phys.* **50** 183001
[81] Zhao C, Wang Q, Lu Y, Jiang L, Liu L, Yu X, Chen L, Li B and Hu Y-S 2019 *Energy Storage Mater.* **20** 395–400
[82] Zhang H L and Song T F 2013 *Electrochim. Acta* **114** 116–24
[83] Li X, Xie Z, Liu W, Ge W, Wang H and Qu M 2015 *Electrochim. Acta* **174** 1122–30
[84] Li X, Kang F, Shen W and Bai X 2007 *Electrochim. Acta* **53** 1761–5
[85] Li L, Song B H, Chang Y L, Xia H, Yang J R, Lee K S and Lu L 2015 *J. Power Sources* **283** 162–70
[86] Kim G H, Kim J H, Myung S T, Yoon C S and Sun Y K 2005 *J. Electrochem. Soc.* **152** A1707–13
[87] Ki Soo Park M H C, Sung J J, Chi H S and Kee S N 2005 *Korean J. Chem. Eng.* **22** 560
[88] Zhang Q, Huang Y, Liu Y, Sun S, Wang K, Li Y, Li X, Han J and Huang Y 2017 *Sci. China Mater.* **60** 629–36
[89] Chen H *et al* 2019 *Electrochim. Acta* **308** 64–73
[90] Liu K *et al* 2020 *Adv. Energy Mater.* **10** 2000135
[91] Wang Y, Wang X, Li X, Yu R, Chen M, Tang K and Zhang X 2019 *Chem. Eng. J.* **360** 139–47

[92] Zhang H *et al* 2015 *J. Electrochem. Soc.* **162** A1899
[93] Chen Z and Dahn J R 2003 *Electrochem. Solid-State Lett.* **6** A221
[94] Zhou Y, Lee Y, Sun H, Wallas J M, George S M and Xie M 2017 *ACS Appl. Mater. Interfaces* **9** 9614–9
[95] Bian X, Fu Q, Bie X, Yang P, Qiu H, Pang Q, Chen G, Du F and Wei Y 2015 *Electrochim. Acta* **174** 875–84
[96] Li C, Zhang H P, Fu L J, Liu H, Wu Y P, Rahm E, Holze R and Wu H Q 2006 *Electrochim. Acta* **51** 3872–83
[97] Lee Y, Mun J, Kim D-W, Lee J K and Choi W 2014 *Electrochim. Acta* **115** 326–31
[98] Lu J, Peng Q, Wang W, Nan C, Li L and Li Y 2013 *J. Am. Chem. Soc.* **135** 1649–52
[99] Cheng H-M, Wang F-M, Chu J P, Santhanam R, Rick J and Lo S-C 2012 *J. Phys. Chem.* C **116** 7629–9637
[100] Zhao J and Wang Y 2012 *J. Phys. Chem.* C **116** 11867–76
[101] Xie J *et al* 2017 *ACS Nano* **11** 7019–27
[102] Ledwoch D *et al* 2020 *Batteries Supercaps* **3** 1–11
[103] Hwang J-Y, Myung S-T, Choi J U, Yoon C S, Yashiro H and Sun Y-K 2017 *J. Mater. Chem.* A **5** 23671–80
[104] Jo J H, Choi J U, Konarov A, Yashiro H, Yuan S, Shi L, Sun Y-K and Myung S-T 2018 *Adv. Funct. Mater.* **28** 1705968
[105] Liu Y, Fang X, Zhang A, Shen C, Liu Q, Enaya H A and Zhou C 2016 *Nano Energy* **27** 27–34
[106] Chen Z, Qin Y, Amine K and Sun Y K 2010 *J. Mater. Chem.* **20** 7606–12
[107] Li N, Ren J, Dang R, Wu K, Lee Y L, Hu Z and Xiao X 2019 *J. Power Sources* **429** 38–45
[108] Dang R, Chen M, Li Q, Wu K, Lee Y L, Hu Z and Xiao X 2019 *ACS Appl. Mater. Interfaces* **11** 856–64
[109] Jo C-H, Jo J-H, Yashiro H, Kim S-J, Sun Y-K and Myung S-T 2018 *Adv. Energy Mater.* **8** 1702942
[110] Hwang J-Y, Yu T-Y and Sun Y-K 2018 *J. Mater. Chem.* A **6** 16854–62
[111] Dang R, Li Q, Chen M, Hu Z and Xiao X 2019 *Phys. Chem. Chem. Phys.* **21** 314–21
[112] Tang K, Huang Y, Xie X, Cao S, Liu L, Liu M, Huang Y, Chang B, Luo Z and Wang X 2020 *Chem. Eng. J.* **384** 123234
[113] Lee E *et al* 2014 *Adv. Energy Mater.* **4** 1400458
[114] Chen C, Han Z, Chen S, Qi S, Lan X, Zhang C, Chen L, Wang P and Wei W 2020 *ACS Appl. Mater. Interfaces* **12** 7144–52
[115] Hwang J Y, Oh S M, Myung S T, Chung K Y, Belharouak I and Sun Y K 2015 *Nat. Commun.* **6** 6865
[116] Guo S, Liu P, Yu H, Zhu Y, Chen M, Ishida M and Zhou H 2015 *Angew. Chem., Int. Ed. Engl.* **54** 5894–9
[117] Li Z-Y, Zhang J, Gao R, Zhang H, Zheng L, Hu Z and Liu X 2016 *J. Phys. Chem.* C **120** 9007–16
[118] Zhou D, Huang W, Lv X and Zhao F 2019 *J. Power Sources* **421** 147–55
[119] Qi X, Liu L, Song N, Gao F, Yang K, Lu Y, Yang H, Hu Y-S, Cheng Z-H and Chen L 2017 *ACS Appl. Mater. Interfaces* **9** 40215–23
[120] Zhou Y-N, Wang P-F, Niu Y-B, Li Q, Yu X, Yin Y-X, Xu S and Guo Y-G 2019 *Nano Energy* **55** 143–50
[121] Yan Z *et al* 2019 *Angew. Chem., Int. Ed. Engl.* **58** 1412–6
[122] Chen X, Zhou X, Hu M, Liang J, Wu D, Wei J and Zhou Z 2015 *J. Mater. Chem.* A **3** 20708–14
[123] Shi W-J, Yan Y-W, Chi C, Ma X-T, Zhang D, Xu S-D, Chen L, Wang X-M and Liu S-B 2019 *J. Power Sources* **427** 129–37
[124] Keller M, Buchholz D and Passerini S 2016 *Adv. Energy Mater.* **6** 1501555
[125] Chagas L G, Buchholz D, Vaalma C, Wu L and Passerini S 2014 *J. Mater. Chem.* A **2** 20263–70
[126] Ju J-H and Ryu K-S 2011 *J. Alloys Compd.* **509** 7985–92
[127] Jun D-W, Yoon C S, Kim U-H and Sun Y-K 2017 *Chem. Mater.* **29** 5048–52
[128] Liang L, Jiang J, Jiang F, Hu G, Cao Y, Peng Z and Du K 2017 *J. Alloys Compd.* **695** 1993–7
[129] Su L, Jing Y and Zhou Z 2011 *Nanoscale* **3** 3967–83
[130] Duan W, Zhu Z, Li H, Hu Z, Zhang K, Cheng F and Chen J 2014 *J. Mater. Chem.* A **2** 8668–75
[131] Yan H, Fu Y, Wu X, Xue X, Li C and Zhang L 2019 *Solid State Ion.* **336** 95–101
[132] Huang Y, Xie M, Wang Z, Jiang Y, Yao Y, Li S, Li Z, Li L, Wu F and Chen R 2018 *Small* **14** e1801246
[133] Okubo M, Li C H and Talham D R 2014 *Chem. Commun.* **50** 1353–5
[134] Wan M, Tang Y, Wang L, Xiang X, Li X, Chen K, Xue L, Zhang W and Huang Y 2016 *J. Power Sources* **329** 290–6
[135] Zhang Q, Fu L, Luan J, Huang X, Tang Y, Xie H and Wang H 2018 *J. Power Sources* **395** 305–13
[136] Xu G-L *et al* 2017 *Energy Environ. Sci.* **10** 1677–93
[137] Sun Y-K, Chen Z, Noh H-J, Lee D-J, Jung H-G, Ren Y, Wang S, Yoon C S, Myung S-T and Amine K 2012 *Nat. Mater.* **11** 942–7
[138] Kim J, Cho H, Jeong H Y, Ma H, Lee J, Hwang J, Park M and Cho J 2017 *Adv. Energy Mater.* **7** 1602559
[139] Cho J, Wang C M, Chan H M, Rickman J M and Harmer M P 2005 *Acta Mater.* **47** 4197–207
[140] Fromhold T M *et al* 2004 *Nature* **428** 726–30
[141] Buban J P, Matsunaga K, Chen J, Shibata N, Ching W Y, Yamamoto T and Ikuhara Y 2006 *Science* **311** 212–5
[142] Luo J, Cheng H, Asl K M, Kiely C J and Harmer M P 2011 *Science* **333** 1730–3
[143] Yan P, Zheng J, Liu J, Wang B, Cheng X, Zhang Y, Sun X, Wang C and Zhang J-G 2018 *Nat. Energy* **3** 600–5
[144] Tepavcevic S *et al* 2020 *Adv. Energy Mater.* **10** 1903128
[145] Su D, Wang C, Ahn H J and Wang G 2013 *Chemistry* **19** 10884–9
[146] Li H, Li J, Ma X and Dahn J R 2018 *J. Electrochem. Soc.* **165** A1038–45